DETECTING HYPERVELOCITY STAR CANDIDATES USING ASTROMETRIC DATA

MINOR RESEARCH PROJECT

Conducted at Leiden Observatory

Under the supervision of Anthony G.A. Brown and Yuri Levin

Tri Laksmana Astraatmadja

Student Number 0646385

astraatmadja@strw.leidenuniv.nl

English Abstract

This project concentrates on developing search criteria to detect hypervelocity stars (HVS) in an astrometric catalogue, in preparation for the upcoming *Gaia* mission. A selection procedure has been developed using the geometrical assumption that HVS move radially away from the Galactic Center. From the proper motion data set we can calculate the Galactocentric-rest frame velocity and the predicted heliocentric radial velocity. The *Hipparcos* Catalogue (ESA, 1997) is used to test the efficiency of this technique.

Hypervelocity stars move at extreme speed ($\gtrsim$1000 km s^{-1}) away from the Galactic Center. They are created through dynamical encounters between close binaries and the supermassive black hole (SMBH) in the Galactic Center. This was first predicted by Hills (1988) and later models by Yu & Tremaine (2003), Gualandris et al. (2005), Levin (2006), and Sesana et al. (2006) confirm this prediction. The first discovery of a HVS, SDSS J090745.0+024507, by Brown et al. (2005) and later six others by Hirsch et al. (2005), Brown et al. (2006a, 2006b), and Edelmann et al. (2005) give credence to all these models. The search program for HVS is motivated by their importance as probes to understand the dynamics within the Galactic Center and by the constraint they provide on the shape and the orientation of the Galactic halo (Gnedin et al. 2005). Brown et al. (2006a, 2006b, 2007) have conducted a successful targeted search for HVS restricted to a specific spectral type, however a thorough search using astrometric data has yet to be done.

The *Gaia* mission, due to be launched no later than 2012, will conduct a complete survey of parallaxes and proper motions for $\sim 10^9$ stars down to $V = 20$. This will present us with an opportunity to search for HVS and study their motion. However, the HVS Catalogue has to be extracted from an enormous data set. We need efficient search criteria to detect HVS within such an astrometric catalogue, to reject as much non-HVS as possible.

Applying the developed criteria to *Hipparcos* yields 3645 HVS candidates, with three different radial velocity catalogues employed to cross-check the predicted radial velocity with the observed

ones. Assuming that these candidates are physically "normal" stars, these candidates are then plotted in the "astrometric" H-R Diagram (Arenou & Luri, 1999) and compared with a set of "good and well-behaved" *Hipparcos* stars. By calculating their proximity to those "good and well-behaved" stars, a ranking of the most plausible down to the least plausible HVS candidates is constructed for later follow-up by actual radial velocity measurements. We conclude that there might only be 210 candidates that can be followed-up with direct observations.

The technique developed in this work is successful in rejecting 96.9% of the considered sample but this percentage is still too low given the expected ratio of HVS to the other stars in the Galaxy. However this technique relies on the distance indicator, but the poorly measured parallaxes can be replaced with a well-calibrated photometric distance, while the technique of comparing HVS candidates with the "good" stars can be refined if we can construct an approximate H-R Diagram for the stellar content of the Galactic Center.

Key words: Astrometry – Catalogues – Galaxy: center – Galaxy: kinematics and dynamics – Galaxy: solar neighbourhood – Stars: kinematics.

Nederlandse Samenvatting

Dit project concentreert zich op het ontwikkeling van zoekcriteria om hogesnelheidsterren (*Hypervelocity Stars* of HVS) te ontdekken in een astrometrische catalogus, als een voorbereiding voor de aankomende *Gaia* missie. Door een geometrische aanname te maken dat hogesnelheidsterren radieel van het Galactisch centrum bewegen, is een selectieprocedure ontwikkeld. Met behulp van de eigenbeweging kunnen wij tevens de galactocentrische snelheid en de voorspelde heliocentrische radiële snelheid uitrekenen. De *Hipparcos* Catalogus (ESA, 1997) wordt gebruikt om de bruikbaarheid van deze technieken te testen.

Hogesnelheidsterren bewegen met een zeer hoge snelheid ($\gtrsim$1000 km s^{-1}) weg van het galactische centrum. Zij worden gecreëerd door dynamische ontmoetingen tussen dichte dubbelsterren met het supermassief zwarte gat in het galactisch centrum. Dit werd als eerste door Hills (1988) voorspeld. Volgende modellen door Yu & Tremaine (2003), Gualandris et al. (2005), Levin (2006), en Sesana et al. (2006) bevestigen deze voorspelling. De eerste ontdekking van een hogesnelheidster, SDSS J090745.0+024507, door Brown et al. (2005), en de volgende zes door Hirsch et al. (2005), Brown et al. (2006a, 2006b), en Edelmann et al. (2005) hechten geloof aan al deze modellen. Het zoekprogramma voor hogesnelheidsterren wordt gemotiveerd dooradat zij hun belangrijk zijn om de dynamica binnen het Galactische Centrum te begrijpen en door de beperking die zij op de vorm en de orientatie van de Galactische halo leggen (Gnedin et al. 2005). Brown et al. (2006a, 2006b, 2007) hebben een succesvol onderzoekprogramma geleid voor het anders van hogesnelheidsterren van een specifiek spectraaltype, maar een volledig zoektocht naar astrometrische parameters moet nog komen.

Het *Gaia* missie, die niet later dan 2012 zal worden gelanceerd, zal leiden tot een kompleet overzicht van parallaxen en eigenbewegingen voor $\sim 10^9$ sterren tot op $V = 20$. Dit geeft ons de kans om naar hogesnelheidsterren te zoeken en hun beweging te bestuderen. Maar de catalogus van hogesnelheidsterren moet worden geëxtraheerd uit een enorme dataset. Wij hebben bruikbare zoekscriteria nodig om hogesnelheidsterren binnen een astrometrische catalogus te

ontdekken, en om zoveel mogelijk niet-hogesnelheidsterren te verwerpen.

Door toepassing van de ontwikkelde criteria op de *Hipparcos* Catalogus kandideren zich 3645 hogesnelheidsterren, hiervoor zijn drie verschillende radiëlesnelheidscatalogi gebruikt om de voorspelde radiële snelheid met de waargenomen radiële snelheden te vergelijken. Verondersteld dat deze kandidaten normale sterren zijn, zijn deze kandidaten geplot in de "astrometrisch" diagram H-R (Arenou & Luri, 1999) en worden ze met een set van "normaal gedragende" sterren vergeleken. Door de afstand te berekenen van de kandidaten tot "normaal gedragende" sterren, wordt een rangschikking gemaakt van de meest aannemelijke naar de minste aannemelijke hogesnelheidsterkandidaten. Deze zullen later worden opgevolgd door metingen van radiële snelheden. Wij concluderen dat er misschien 210 kandidaten zonden kunnen zijn, die met directe observaties kunnen worden opgevolgd.

Door de technieken die in dit project zijn ontwikkeld, kunnen 96.9% van het genomen sample verworpen worden, maar dit percentage is nog te klein voor het verwachte percentage van hogesnelheidsterren in de Melkweg. Omdat deze technieken afhangen van de afstandsindicator, kunnen de slecht gemeten parallaxen dan met een goed-gekalibreerde photometrische afstand worden vervangen. Verder kan de techniek om hogesnelheidsterkandidaten met de "goede" sterren te vergelijken worden verfijnd als wij een benaderend H-R Diagram voor de stellaire inhoud van het Galactische Centrum kunnen construeren.

Sleutelwoorden: Astrometrie – Catalogus – Melkweg: centrum – Melkweg: kinematica en dynamica – Melkweg: nabije omgeving – Sterren: kinematica.

Abstrak Bahasa Indonesia

Pekerjaan ini dikonsentrasikan pada pengembangan kriteria pencarian bintang hipercepat (*hypervelocity star* atau HVS) dalam sebuah katalog astrometri, sebagai persiapan untuk misi *Gaia* yang akan datang. Serangkaian prosedur seleksi telah dikembangkan dengan menggunakan asumsi geometris bahwa bintang hipercepat bergerak dalam arah radial menjauhi Pusat Galaksi. Dari set data gerak diri dapat ditentukan kecepatannya relatif terhadap Pusat Galaksi dan juga prediksi terhadap kecepatan radial heliosentriknya. Katalog *Hipparcos* (ESA, 1997) digunakan untuk menguji efisiensi teknik-teknik ini.

Bintang hipercepat bergerak dengan kecepatan ekstrim ($\gtrsim$1000 km s^{-1}) menjauhi Pusat Galaksi. Mereka tercipta dari perjumpaan *(encounter)* dinamik antara bintang-bintang ganda dekat dengan Lubang Hitam Supermasif di Pusat Galaksi. Ini diprediksi pertama kali oleh Hills (1988) dan model-model selanjutnya oleh Yu & Tremaine (2003), Gualandris et al. (2005), Levin (2006), dan Sesana et al. (2006) mengkonfirmasi prediksi ini. Penemuan pertama sebuah bintang hipercepat, SDSS J090745.0+024507, oleh Brown et al. (2005) dan kemudian enam lainnya oleh Hirsch et al. (2005), Brown et al. (2006a, 2006b), dan Edelmann (2005) memantapkan prediksi ini. Diadakannya program pencarian bintang hipercepat dimotivasi oleh pentingnya peran bintang hipercepat dalam memahami dinamika di daerah sekitar Pusat Galaksi dan juga untuk memberikan batasan-batasan pada bentuk dan orientasi Halo Galaktik (Gnedin et al. 2005). Brown et al. (2006a, 2006b, 2007) dengan sukses telah melakukan pencarian terseleksi untuk bintang-bintang dengan kelas spektrum tertentu, namun hingga kini belum ada pencarian menyeluruh melalui paramater-parameter astrometri.

Misi *Gaia*, direncanakan untuk diluncurkan sebelum pertengahan 2012, akan melakukan survey terhadap paralaks dan gerak diri dari $\sim 10^9$ bintang lengkap hingga $V = 20$ magnitudo. Ini akan memungkinkan kita mencari bintang hipercepat dan mempelajari gerak mereka, namun katalog bintang hipercepat yang ingin kita hasilkan harus diekstraksi dari set data berjumlah teramat besar. Dibutuhkan kriteria pencarian yang efektif untuk mendeteksi bintang hipercepat

dalam katalog astrometri seperti demikian, untuk dapat menolak sebanyak mungkin bintang-bintang non-hipercepat.

Aplikasi kriteria yang telah dikembangkan pada Katalog *Hipparcos* menghasilkan 3645 kandidat, dengan menggunakan pula tiga katalog kecepatan radial sebagai pemeriksaan silang antara kecepatan radial yang diprediksi dengan yang diamati. Dengan menganggap kandidat ini adalah bintang-bintang yang secara fisik "normal", kandidat-kandidat ini dipetakan dalam Diagram H-R "astrometris" (Arenou & Luri, 1999) untuk dibandingkan dengan set data bintang-bintang *Hipparcos* yang "berkelakuan baik." Dengan menentukan seberapa jauh kandidat-kandidat ini dari bintang-bintang "berkelakuan baik" tersebut, dapat disusun peringkat kandidat bintang hipercepat dari yang paling mungkin hingga yang paling tidak mungkin, sehingga bintang-bintang ini dapat ditindaklanjuti melalui pengukuran kecepatan radial. Teknik ini menyimpulkan bahwa kemungkinan hanya ada 210 kandidat yang layak ditindaklanjuti.

Teknik yang dikembangkan dalam pekerjaan ini berhasil membuang 96.9% sampel *Hipparcos* namun ini masih terlalu kecil bila melihat ekspektasi jumlah bintang hipercepat relatif terhadap jumlah bintang di Galaksi. Karena teknik ini bergantung pada indikator jarak, paralaks berkualitas rendah dapat diganti dengan jarak fotometrik yang telah terkalibrasi dengan baik, sementara pembandingan kandidat bintang hipercepat dengan bintang-bintang "berkelakuan baik" dapat diperbaiki bila kita dapat menyusun Diagram H-R untuk bintang-bintang di Pusat Galaksi.

kata kunci: Astrometri – Katalog – Galaksi: pusat – Galaksi: kinematika dan dinamika – Galaksi: daerah lokal matahari – bintang: kinematika.

Contents

List of Tables

List of Figures

Chapter 1

Introduction

It is believed that in the center of the Galaxy lies a massive black hole (BH) with a mass of the order of $2 \times 10^6 M_\odot$ (Binney & Merrifield, 1998). Hills (1988) has calculated that a close encounter between a tightly bound binary with the BH can cause one binary component to be bounded to the BH while the other will be ejected from the Galactic center with a speed of up to 4000 km s^{-1}. The latter were named hypervelocity stars (HVS). The discovery of even one such HVS can provide a definitive evidence for the existence of such a massive BH in the Galactic center, because no other known mechanism can produce such a star. Hills calculated that one HVS with $V = 1400$ km s^{-1} is ejected from the Galactic center every 10^3 yr, which means that we can expect as least 6000 HVS within the solar circle.

Yu & Tremaine (2003) later provide two additional mechanisms to eject HVS from the Galactic center: gravitational encounters of two single stars and a three-body encounter between a single star and a binary black hole (BBH). They predict that 1) the rate of ejection for an encounter between two stars is 10^{-11} yr^{-1}, which is too low to be detectable and hence negligible, and 2) also in agreement with Hills, we can expect $\sim 10^3$ HVS within the solar circle. This makes HVS extremely rare and hard to find since we can expect at the order of 10^{11} stars within the solar circle. Gualandris et al. (2005) studied the ejection mechanism by a supermassive black hole (SMBH) through scattering experiments and found that tidal disruption of binaries will create HVS with higher velocities while BBH eject HVS at a higher rate. Levin (2006) found that in the case of an inspiraling intermediate-mass black hole (IMBH) toward a SMBH, the inspiraling IMBH will eject HVS in a burst that lasts a few dynamical friction timescales, and that most of the stars will be ejected isotropically. If the orbit of the IMBH is eccentric, the ejected stars will form a broad "jet" roughly aligned with the pericenter velocity of the IMBH.

Sesana et al. (2006) also obtained the same result with their experiments of full three-body scattering: black holes with eccentric orbits eject HVS along a broad jet perpendicular to the semimajor axis.

Not only are HVS important to prove the existence of a BH (or BBH) in the Galaxy and to understand the dynamics in the Galactic Center, but they are also important probes of multi-scale Galactic phenomena. Gnedin et al. (2005) showed that knowledge of the trajectories of HVS would give significant constraints on the shape and orientation of the Galactic halo. Their frequency of ejection, spectral properties, and distribution can provide important constraints on star formation in the Galactic Center (Kollmeier & Gould, 2007). It is thus important to start developing a search program to look for HVS.

In 2005, in a kinematic survey of blue horizontal branch (BHB) stars, Brown et al. (2005) serendipitously discovered the first HVS, SDSS J090745.0+024507, travelling with a heliocentric radial velocity of 853 ± 12 km s^{-1}, and a Galactocentric velocity of at least 709 km s^{-1}. Because the star is either a BHB or a B9 main sequence star, its heliocentric distance can be either 39 or 71 kpc, respectively. At the HVS' mean distance of 55 ± 16 kpc, the mass of the Galaxy is $5.4 \times 10^{11} M_{\odot}$ and its escape velocity is $v_{\rm esc} = 305$ km s^{-1}. Hence the HVS is moving with well over twice the escape velocity from the Galaxy and is unbound to the Galactic potential. Gualandris et al. (2005) traced back the star's trajectory in the Galactic potential and found that it should have a proper motion of 2 mas yr^{-1} if it came from within a few parsecs from the SMBH. Recent observation by Fuentes et al. (2006) showed the HVS to be a low-amplitude variable. They resolved its spectral type to be a B9 main sequence star, and concluded its distance to be 71 kpc from the Sun.

At present, 6 HVS ejected from the Galaxy have been discovered by Brown et al. (2005, 2006a) and also by Hirsch et al. (2005) in a survey of subluminous O stars, while 1 HVS, discovered by Edelmann et al. (2005) in their survey of subluminous B stars (sdB), is thought to be ejected from the Large Magellanic Cloud. All initially discovered HVS were contaminants in a survey of blue stars. Following the discovery of the first HVS, Brown et al. (2006a, 2006b, 2007) conducted the first targeted search of HVS by selecting B-type stars in the Sloan Digital Sky Survey (SDSS) and not only did they successfully discover 4 new HVS but also a new class of HVS: bound HVS that were moving at high velocity but are still gravitationally bounded to the Galaxy. The survey also observed that HVS have a marginally anisotropic distribution at 2σ confidence toward the anticenter hemisphere (Brown et al. 2007). Table 1.1 summarises the properties of all the known seven HVS so far.

Table 1.1: Properties of hyper-velocity stars that has been discovered so far, taken from Brown et al. (2006b). The columns are HVS number, Galactic coordinates (l, b), apparent magnitude g' (g' are one of SDSS' broad-band photometric system, with effective wavelength $\lambda_{\rm eff}$ = 480 nm and FWHM = 141 nm, approximately halfway between the Johnson-B and V systems), minimum Galactocentric rest-frame velocity v_{rf} (not a full space velocity), estimate of heliocentric distance d, estimated travel time $t_{\rm GC}$ since its ejection, Catalogue name, and the reference.

ID	l	b	g'	v_{rf}	d	$t_{\rm GC}$	Catalogue Name	Ref.
	$^\circ$	$^\circ$	mag	km s^{-1}	kpc	Myr		
HVS1	227.3	31.3	19.8	+709	71	160	SDSS J090745.0+024507	1
HVS2	176.0	47.1	18.8	+717	19	32	US 708	2
HVS3	263.0	40.9	16.2	+548	61	100	HE 04375439	3
HVS4	194.8	42.6	18.4	+563	75	130	SDSS J091301.0+305120	4
HVS5	146.3	38.7	17.9	+643	55	90	SDSS J091759.5+672238	4
HVS6	243.1	59.6	19.1	+508	75	160	SDSS J110557.45+093439	4
HVS7	263.8	57.9	17.7	+418	55	120	SDSS J113312.12+010824.9	4

References: (1) Brown et al. 2005, (2) Hirsch et al. 2005, (3) Edelmann et al. 2005, (4) Brown et al. 2006a.

All discovered HVS so far are blue stars and this reflects the fact that they are discovered in a survey of blue stars or through a preselected target of blue stars. A search using astrometric data is currently not feasible since no astrometric catalogue has gone deep enough. If we assume that a HVS is solar-type star with $M_V = 4.77$, then at a distance of 10 kpc from us its V-band apparent magnitude is $V = 19.77$, its parallax is $\varpi = 0.1$ mas and its proper motion is $\mu \sim 21$ mas yr^{-1} if it is moving with a tangential velocity of $v_T = 1000$ km s^{-1}. Although the proper motion is still within the limit of reasonable accuracy, the magnitude is beyond the limiting magnitude of any astrometric catalogue, including the *Hipparcos* Catalogue with a limiting magnitude of 12.4. No astrometric survey has measure such a small parallax with sufficient accuracy either. But in the future this will no longer be the case. The *Gaia* satellite mission, a more ambitious successor to *Hipparcos*, is now in preparation. In October 2000, *Gaia* was selected as the 6th Cornerstone of the European Space Agency (ESA) Horizon 2000+ programme and it will be launched no later than 2012. It aims to create a precise three-dimensional map of 1 billion stars in the Galaxy and beyond, as well as to measure their motions. To achieve this, *Gaia* will accurately measure the positions, parallaxes, and proper motions of all stars down to the limiting magnitude of $V = 20$

Table 1.2: A summary of *Gaia*'s survey and measurement capabilities. μas is micro-arcsecond.

Survey parameters	
Magnitude limit	20 – 21 mag
Completeness	$V = 20$ mag
Number of objects	26×10^6 to $V = 15$ mag
	250×10^6 to $V = 18$ mag
	10^9 to $V = 20$ mag
Measurement and accuracies	
parallax	7μas at $V = 10$ mag
	$12 - 25\mu$as at $V = 15$ mag
	$100 - 300\mu$as at $V = 20$ mag
photometry	low resolution
	prism spectra to $V = 20$ mag
radial velocities	$1 - 15$ km s^{-1} to $V = 17$ mag

as well as radial velocities for all stars brighter than $V \simeq 17$ magnitude. *Gaia* will also measure the photometric properties of each detected objects and an on-board object detection scheme is developed to ensure a complete census of every object with $V \leq 20$ magnitude. A summary of *Gaia*'s capabilities are given in Table 1.2. These astrometric accuracies is then put into a model of the Galaxy to calculate the distance and an assessment of the corresponding relative errors in distance and parallax (Perryman et al. 2001). 2 million stars will have distance accuracies to better than 1 percent, 50 million better than 2 percent, 110 million better than 5 percent, and 220 million better than 10%. 40 million stars will have tangential velocity accuracies to better than 0.5 km s^{-1}, 80 million better than 1 km s^{-1}, 200 million better than 3 km s^{-1}, 300 million better than 5 km s^{-1}, and 440 million better than 10 km s^{-1}. Note that although the absolute errors are magnitude-depended, the relative errors in distance depend on the actual distance to the stars. Hence faint and faraway stars will still pose a problem to accurately estimate their distance.

The challenge will be to detect HVS within such an enormous amount of data at varying levels of accuracy. Nearby HVS within 1 kpc, should there be any, might be easily detected because up to this distance, astrometric parameters are accurately measured, but the real challenge is to be able to unambiguously detect fainter and farther HVS within the larger volume of

Gaia's detection sphere. We will need to develop search criteria that will enable us to extract a subsample of *Gaia* containing HVS. The goal of this project is to exploit our current knowledge on the kinematics of HVS to devise preliminary criteria that will reject as much non-HVS as possible, and then investigate whether any other method involving photometry can reject more stars.

As a first step, we make an a priori assumption that all stars are HVS. We then construct a kinematical model assuming that HVS only move radially away from the Galactic center. From the proper motion we can then calculate its supposed distance and compare it with the observed distance. We also calculate its Galactocentric-rest frame velocity to see whether it is fast enough to be considered a HVS. This will be described in the next chapter, Chapter 2. In Chapter 3, we apply these criteria to the *Hipparcos* Catalogue and discuss the resulting subsample. For a large number of candidates the predicted distance would make their luminosities too bright in the H-R Diagram. Hence a further selection was done by comparing the candidates' inferred locations on the H-R Diagram with ordinary stars from the *Hipparcos* Catalogue in order to narrow down the list of stars to be followed-up. A ranking is constructed based on their proximity to ordinary stars, and a priority-based observing list is produced. A discussion of the results and future work will appear in Chapter 4.

Chapter 2

Kinematics of HVS

2.1 Basic assumptions

In this work two assumptions on the kinematics of HVS are taken. The first one is that HVS move in a radial direction away from the Galactic Center without any movement in the tangential direction. This is a distinct kinematical feature of a HVS, although there should be small changes induced by the nonspherical component of the Galactic potential (Yu & Tremaine, 2003). Since only HVS moving at more than 10^3 km s^{-1} are considered, which is well over the local escape speed from the Galaxy, then this small perturbation is negligible. Secondly, it is assumed that all stars lack radial velocity data to begin with, and we have to work only with proper motions and parallaxes. This is a valid assumption since only 20% of stars in the *Hipparcos* Catalogue have radial velocity data and this is limited only to the brightest stars. Furthermore there will be only 100 – 150 million stars out of ∼1 billion stars that will be surveyed by *Gaia* that will have radial velocity data. In either case it is better to work only with the astrometric data.

2.2 Kinematical model of HVS

The position and motions of stars relative to the Sun are all described in the Galactic coordinate system as well as within the Cartesian frame of reference with the same orientation as the Galactic coordinate systems, and centered on the Sun. The Galactic coordinate system along with the useful transformations from Equatorial to Galactic coordinates are all described in Appendix A. Let us now consider an arbitrary HVS in the direction (l, b) at a distance $d = 1/\varpi$ moving radially away from the Galactic Center, where ϖ is the star's parallax angle. The Galactocentric-rest frame velocity vector is $v_{RF}\hat{\mathbf{r}}'$, where $\hat{\mathbf{r}}'$ is the unit vector pointing radially

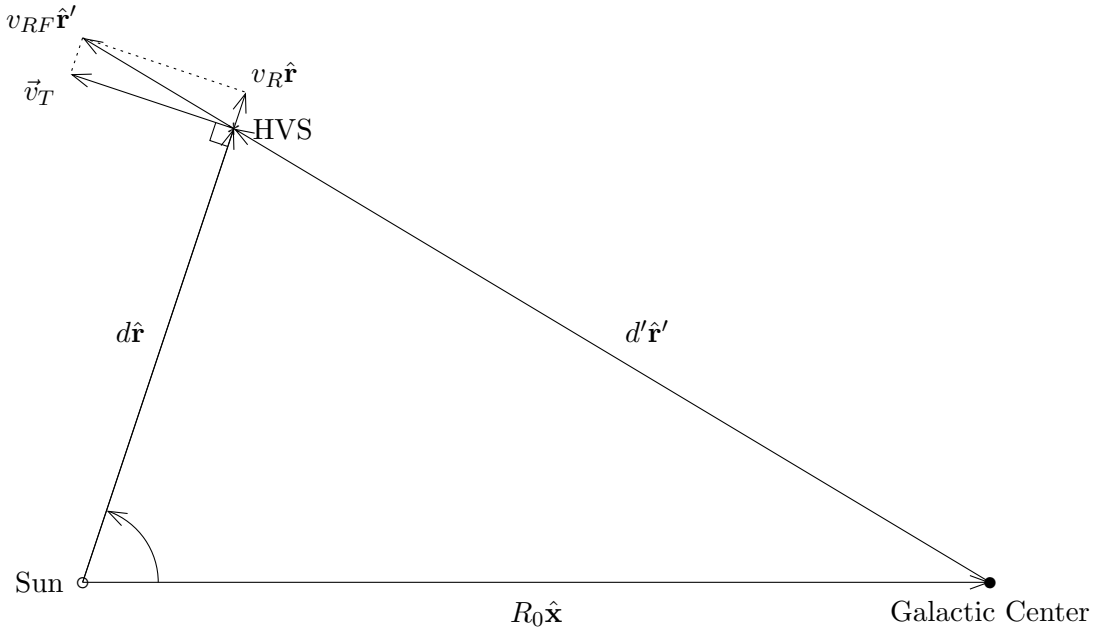

Figure 2.1: The kinematical situation of a HVS. $d\hat{\mathbf{r}}$ is the vector from the Sun to the HVS, $R_0\hat{\mathbf{x}}$ is the vector from the Sun to the Galactic Center (GC), and $d'\hat{\mathbf{r}}'$ is the vector from the GC to the HVS. The rest-frame velocity can be broken-down into the line-of-sight velocity or the radial velocity v_R, the tangential velocity $v_T = \frac{A_v}{\varpi}\sqrt{\mu_{l*}^2 + \mu_b^2}$, and the correction for solar motion.

away from the Galactic center, it can be broken-down into its heliocentric components and the correction for solar motion:

$$v_{RF}\hat{\mathbf{r}}' = v_R\hat{\mathbf{r}} + \frac{A_v}{\varpi}\vec{\mu} + \mathbf{v}_\odot, \tag{2.1}$$

where $v_R\hat{\mathbf{r}}$ is the observed heliocentric radial velocity vector of the star, $A_v = 4.740$ km yr s^{-1}, $\vec{\mu} = \mu_{l*}\hat{\mathbf{p}} + \mu_b\hat{\mathbf{q}}$ is the observed proper motion vector of the star, and $\mathbf{v}_\odot$ is the velocity vector of the solar motion and the circular velocity of the LSR at the solar radius $R_0 = 8.5$ kpc. For this work the standard value of $v_c = 220$ km s^{-1} for the circular velocity of the LSR around the Galactic Center as well as Dehnen & Binney's (1998) values of the solar motion are used:

$$\begin{aligned} v_{\odot,x} = U_0 &= 10.00 \pm 0.36 \text{ km s}^{-1}, \\ v_{\odot,y} - v_c = V_0 &= 5.25 \pm 0.62 \text{ km s}^{-1}, \\ v_{\odot,z} = W_0 &= 7.17 \pm 0.38 \text{ km s}^{-1}. \end{aligned} \tag{2.2}$$

If we take the cross product of $\hat{\mathbf{r}}$ and $\hat{\mathbf{x}}$, we will have a vector perpendicular to both, $\mathbf{e}_\perp = (\hat{\mathbf{r}} \times \hat{\mathbf{x}})$. The dot product of $\hat{\mathbf{r}}'$ and $\mathbf{e}_\perp$ will be zero since both of these vectors are perpendicular to each other. Thus we will have $(\hat{\mathbf{r}}' \cdot \mathbf{e}_\perp) = 0$ as well as $(\hat{\mathbf{r}} \cdot \mathbf{e}_\perp) = 0$. If The Sun is stationary

relative to the GC, Equation 2.1 will simply be $v_{RF}\hat{\mathbf{r}}' = v_R\hat{\mathbf{r}} + \frac{A_v}{\varpi}\vec{\mu}$, and taking the product of both side with $\mathbf{e}_\perp$ will yield $(\vec{\mu}\cdot\mathbf{e}_\perp) = 0$ or

$$\frac{\mu_{l*}}{\mu_b} = \frac{\tan l}{\sin b}. \tag{2.3}$$

The left side of Equation 2.3 is the direction angle of the proper motion vector, while the right side is the direction angle from the GC to the star. Hence if The Sun is stationary then it is easy to notice any star moving radially away from the Galactic Center, we just have to trace back their proper motion vector in the celestial sphere and if it passes the direction to the Galactic Center then the star should came from there. However the solar motion complicates the issue because from our frame of reference it will change the direction vector of the star's movement, and this change depends on the star's distance from the Sun. If we now include the solar motion we will have:

$$\begin{aligned} 0 &= v_R(\hat{\mathbf{r}}\cdot\mathbf{e}_\perp) + \frac{A_v}{\varpi}(\vec{\mu}\cdot\mathbf{e}_\perp) + (\mathbf{v}_\odot\cdot\mathbf{e}_\perp), \\ 0 &= \frac{A_v}{\varpi}(\vec{\mu}\cdot\mathbf{e}_\perp) + (\mathbf{v}_\odot\cdot\mathbf{e}_\perp), \\ \varpi &= -A_v\frac{(\vec{\mu}\cdot\mathbf{e}_\perp)}{(\mathbf{v}_\odot\cdot\mathbf{e}_\perp)}. \end{aligned} \tag{2.4}$$

Thus, given the proper motion of a star, Equation 2.4 tells us the distance where the star has to be put from the Sun, if it is a HVS. Hence this kinematic model has an a priori assumption that all stars are HVS. We could then calculate its supposed parallax then compare this computed parallax ϖ_c with its observed parallax ϖ_{obs} to see whether both agree. If both agree within their errors, then the model is true for the evaluated star and thus it is a HVS.

To compute the magnitude of v_{RF} without any knowledge at all of the observed radial velocity we project $v_{RF}\hat{\mathbf{r}}'$ onto the plane containing the proper motion vector:

$$\begin{aligned} v_{RF}\hat{\mathbf{r}}'\cdot(\hat{\mathbf{p}}+\hat{\mathbf{q}}) &= v_R\hat{\mathbf{r}}\cdot(\hat{\mathbf{p}}+\hat{\mathbf{q}}) + \frac{A_v}{\varpi}\vec{\mu}\cdot(\hat{\mathbf{p}}+\hat{\mathbf{q}}) + \mathbf{v}_\odot\cdot(\hat{\mathbf{p}}+\hat{\mathbf{q}}), \\ v_{RF} &= \frac{v_l + v_b + \mathbf{v}_\odot\cdot\hat{\mathbf{p}} + \mathbf{v}_\odot\cdot\hat{\mathbf{q}}}{\hat{\mathbf{r}}'\cdot\hat{\mathbf{p}} + \hat{\mathbf{r}}'\cdot\hat{\mathbf{q}}}. \end{aligned} \tag{2.5}$$

Since the line of sight vector $\hat{\mathbf{r}}$ is perpendicular to the proper motion vector $\vec{\mu}$, the radial velocity components is once again cancelled. $v_l = \frac{A_v}{\varpi}\mu_{l*}$ and $v_b = \frac{A_v}{\varpi}\mu_b$ are the tangential velocity in the direction of l and b, respectively. This calculation of the total velocity will enable us to test whether the star in question is fast enough to be considered a HVS.

Furthermore, by projecting $v_{RF}\hat{\mathbf{r}}'$ onto the line of sight vector $\mathbf{r}$, we can predict the observed radial velocity:

$$v_{RF}(\hat{\mathbf{r}}'\cdot\hat{\mathbf{r}}) = v_R + \vec{\mathbf{v}}_\odot\cdot\hat{\mathbf{r}},$$

$$v_R = (v_{RF}\hat{\mathbf{r}}' - \vec{\mathbf{v}}_\odot)\cdot\hat{\mathbf{r}}. \tag{2.6}$$

This time $\vec{\mu}$ vanishes because it is perpendicular to $\hat{\mathbf{r}}$. This prediction can be used as a further test should the star in question has an observed radial velocity that we can compare to the prediction.

We can now evaluate Equation 2.4, 2.5, and 2.6 if we know the star's proper motion in the direction of (l, b), its parallax angle ϖ, and all the unit vectors in those equations. The matrix in Equation A.10 in Appendix A tells us that

$$\hat{\mathbf{p}} = -\hat{\mathbf{x}}\sin l + \hat{\mathbf{y}}\cos l, \tag{2.7}$$

$$\hat{\mathbf{q}} = -\hat{\mathbf{x}}\cos l\sin b - \hat{\mathbf{y}}\sin l\sin b + \hat{\mathbf{z}}\cos b, \tag{2.8}$$

$$\hat{\mathbf{r}} = \hat{\mathbf{x}}\cos l\cos b + \hat{\mathbf{y}}\sin l\cos b + \hat{\mathbf{z}}\sin b, \tag{2.9}$$

Thus it is easy to compute

$$\vec{\mathbf{e}}_\perp = \hat{\mathbf{r}}\times\hat{\mathbf{x}} = \begin{vmatrix} \hat{\mathbf{x}} & \hat{\mathbf{y}} & \hat{\mathbf{z}} \\ \cos l\cos b & \sin l\cos b & \sin b \\ 1 & 0 & 0 \end{vmatrix} = \hat{\mathbf{y}}\sin b - \hat{\mathbf{z}}\sin l\cos b, \tag{2.10}$$

$$\begin{aligned} \vec{\mu} &= \mu_{l*}\hat{\mathbf{p}} + \mu_b\hat{\mathbf{q}} \\ &= -\hat{\mathbf{x}}(\mu_{l*}\sin l + \mu_b\cos l\sin b) + \hat{\mathbf{y}}(\mu_{l*}\cos l - \mu_b\sin l\sin b) + \hat{\mathbf{z}}(\mu_b\cos b), \end{aligned} \tag{2.11}$$

$$\hat{\mathbf{r}}' = \frac{\vec{\mathbf{r}} - \vec{\mathbf{R}}_0}{\|\vec{\mathbf{r}} - \vec{\mathbf{R}}_0\|} = \frac{1}{d'}(d\hat{\mathbf{r}} - R_0\hat{\mathbf{x}}), \tag{2.12}$$

where $d' = (d^2 + R_0^2 - 2dR_0\cos l\cos b)^{1/2}$ is the distance from the star to the Galactic Center and $d = 1/\varpi$ is the distance from the Sun to the star. With these equations in hand, the computed parallax angle ϖ_c in Equation 2.4 then becomes

$$\varpi_c = A_v\frac{\mu_b\sin l - \mu_{l*}\cos l\sin b}{v_{\odot,y}\sin b - v_{\odot,z}\sin l\cos b}, \tag{2.13}$$

the Galactocentric rest-frame velocity is

$$v_{RF} = \frac{d'}{R_0}\left(\frac{v_l + v_b + \mathbf{v}_\odot\cdot(\hat{\mathbf{p}} + \hat{\mathbf{q}})}{\sin l + \cos l\sin b}\right), \tag{2.14}$$

and finally, the predicted heliocentric radial velocity is

$$v_R = \frac{v_{RF}}{d'}(d - R_0\cos l\cos b) - (v_{\odot,x}\cos l\cos b + v_{\odot,y}\sin l\cos b + v_{\odot,z}\sin b). \tag{2.15}$$

2.3 The error propagation

It is assumed that the errors in the measurement of equatorial coordinates are small and negligible, so only the errors in parallax and proper motion in equatorial coordinates are considered. Since the proper motion in galactic coordinates consist of the components of proper motion in equatorial coordinates, then their error has a correlation which we must take into account.

To calculate the errors of proper motion in galactic coordinates and their correlations, first we use Equation A.6 in Appendix A to transform the proper motions into the Galactic coordinate system, and calculate the Jacobian **J**. We then calculate the errors of proper motion in Galactic coordinates by means of covariance matrix:

$$\begin{bmatrix} \sigma^2_{\mu_{l*}} & \rho\sigma_{\mu_{l*}}\sigma_{\mu_b} \\ \rho\sigma_{\mu_{l*}}\sigma_{\mu_b} & \sigma^2_{\mu_b} \end{bmatrix} = \mathbf{J} \begin{bmatrix} \sigma^2_{\mu_{\alpha*}} & \rho\sigma_{\mu_{\alpha*}}\sigma_{\mu_\delta} \\ \rho\sigma_{\mu_{\alpha*}}\sigma_{\mu_\delta} & \sigma^2_{\mu_\delta} \end{bmatrix} \mathbf{J}^T \tag{2.16}$$

Now, from Equation 2.13 we can compute the error of the predicted parallax angle by the equation for the propagation of error. We can see that there is a linear relation between ϖ_c and the proper motion components μ_{l*} and μ_b. We can write Equation 2.13 as

$$\varpi_c = c_1\mu_{l*} + c_2\mu_b, \tag{2.17}$$

where

$$c_1 = -A_v \frac{\cos l \sin b}{v_{\odot,y}\sin b - v_{\odot,z}\sin l \cos b}, \tag{2.18}$$

$$c_2 = A_v \frac{\sin l}{v_{\odot,y}\sin b - v_{\odot,z}\sin l \cos b}. \tag{2.19}$$

With the propagation of error equation (Equation B.9), the error in ϖ_c is then

$$\sigma^2_{\varpi_c} = c_1^2\sigma^2_{\mu_{l*}} + c_2^2\sigma^2_{\mu_b} + 2c_1c_2\mathrm{cov}(\mu_{l*}\mu_b), \tag{2.20}$$

where $\mathrm{cov}(\mu_{l*}\mu_b) = \rho\sigma_{\mu_{l*}}\sigma_{\mu_b}$.

Chapter 3

Selecting HVS Candidates

3.1 Preliminary criteria and its application to Hipparcos

In Chapter 2 the geometrical situation of a HVS and its kinematical properties has been showed. Now we will use these properties as a preliminary criteria. As a test for this criteria the *Hipparcos* Catalogue, at present is still the the best available astrometric catalogue, is used. Containing 118 218 stars with median astrometric precision to around 1 mas, it also contains $\sim$ 60 000 objects complete to $V = 7.3 - 9$ (ESA 1997, vol. 1, p. 3–4). This catalogue is also used because of its resemblance to the upcoming *Gaia* mission, which is going to be the successor of *Hipparcos*. For all stars in *Hipparcos*, two kinematical parameters in the HVS model is calculated: observed parallax ϖ_c using Equation 2.4 and Galactocentric velocity v_{RF} using Equation 2.5. The first thing to do is rejecting all stars with $\varpi_c \leq 0$, since these values are meaningless. A negative ϖ_c means that the star has to be put on the opposite side of the sky where we observed it, if it is a HVS. Since that is not the direction where we observed it then this value is meaningless. The same also goes for stars with exactly zero parallax, which means that the star has to be put at infinite distance. However, negative value in observed parallax $\varpi_{\rm obs}$ is acceptable, since these are only stars with low quality in parallax measurement. Afterwards, we could check whether the computed parallax agrees with the observed one. We can do this by looking at the differences between the two and see whether they agree with each other within their errors. We define the dimensionless quantity z, given by

$$z = \frac{\varpi_{\rm obs} - \varpi_c}{\sqrt{\sigma^2_{\varpi_{\rm obs}} + \sigma^2_{\varpi_c}}}, \tag{3.1}$$

which measures how close a particular star is to the kinematical model of an HVS, within the resultant errors in $\varpi_{\rm obs}$ and ϖ_c. If our a priori assumption that "all stars within *Hipparcos*

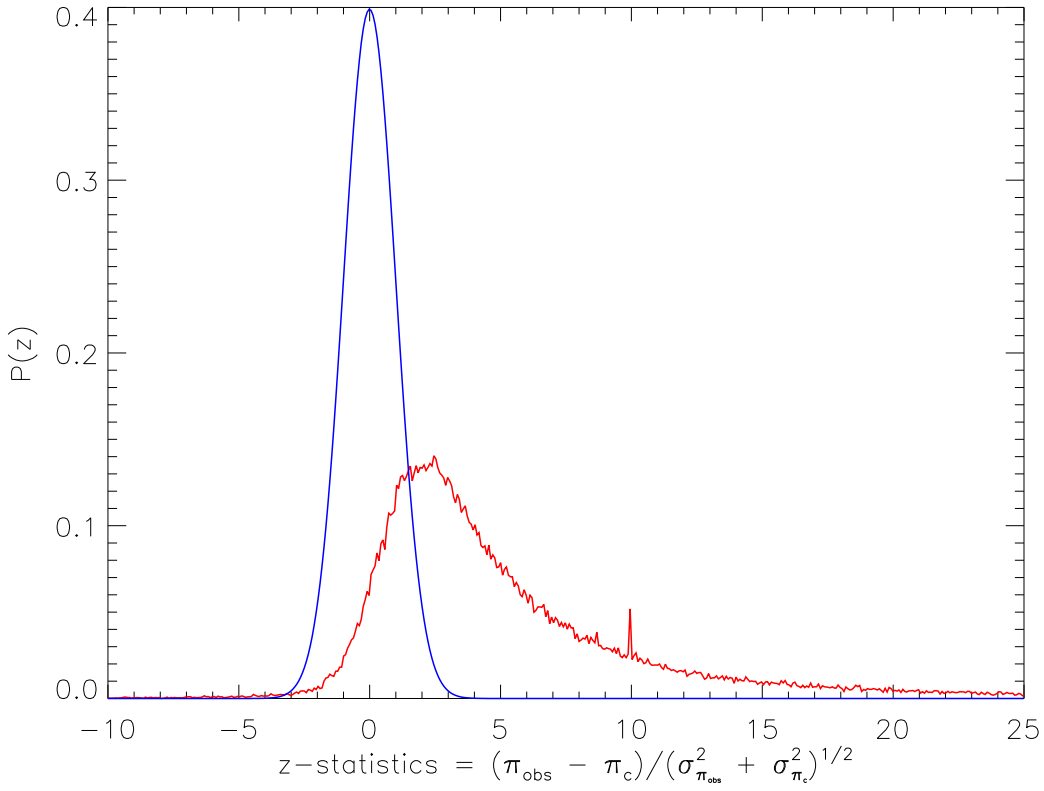

Figure 3.1: The probability density function (PDF) of z (red curve) for all *Hipparcos* stars, compared with a Gaussian PDF (blue curve) with zero mean and unit variance. The large deviation of the z PDF from the Gaussian PDF clearly shows that the kinematical model of HVS is not correct for most of stars.

are HVS" is correct, then the distribution of z should be Gaussian with zero mean and unit variance and errors would only come from measurement errors. However, we know that this is not correct because the majority of stars that we observed don't behave like a HVS. As a test, we can calculate z for all stars in *Hipparcos* and calculate their probability density function (PDF) and compare them with a Gaussian PDF with zero mean and unit variance, shown in Figure 3.1. The blue-coloured curve in Figure 3.1 is the Gaussian probability density function (PDF) of z if all stars are HVS, while the red-coloured curve is the PDF of z for all stars in *Hipparcos*. This departure from a Gaussian distribution is understandable because we are forcing all stars to be HVS and this model is, of course, not true for most cases. For a genuine HVS there is a 99.73% chance that it will have $|z| \leq 3$. Thus, if we reject every *Hipparcos* stars with $|z| \geq 3$, we only reject 0.27% of stars that might be genuine HVSs. This cut-off then has a low false rejection rate since there is only a 0.27% chance of throwing away any real HVS stars.

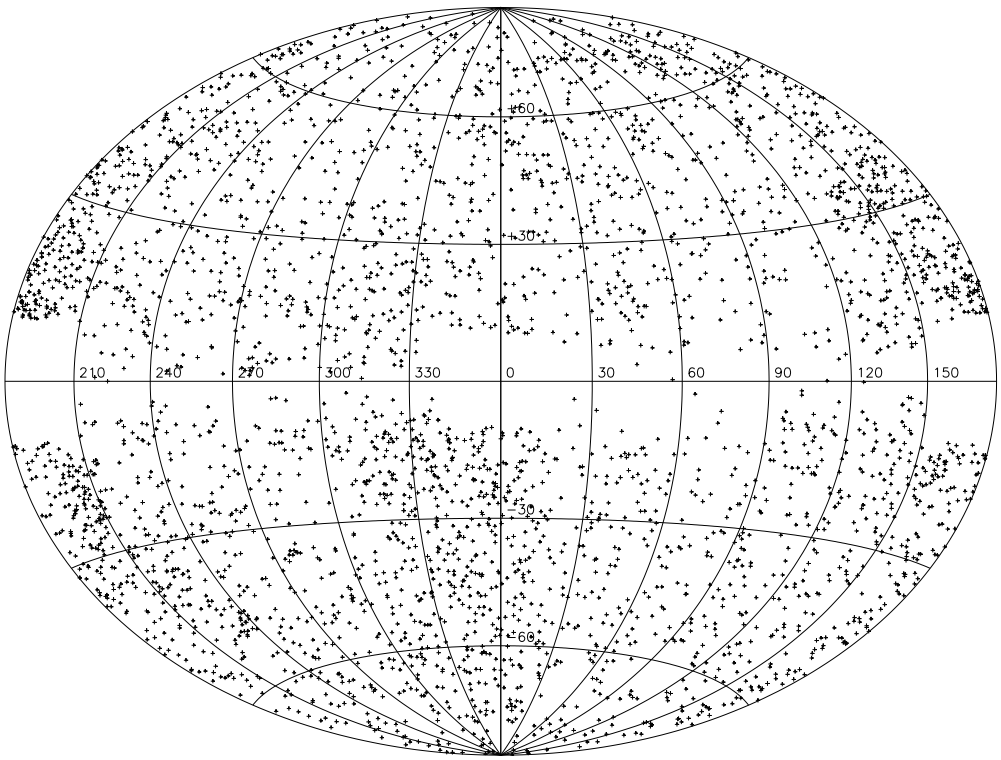

Figure 3.2: The spatial distribution of 3645 HVS candidates in Galactic Coordinates. The center of the plot is the direction of the Galactic Center

The next criterion is to see whether their Galactocentric velocity is fast enough to be considered a hypervelocity stars. The Galactocentric velocity is calculated using computed parallax ϖ_c in Equation 2.5 and checked whether it is higher than 1000 km s^{-1}. The fourth criterion, the stars lying around the direction of the Galactic Center and the Anticenter are rejected. This criterion arise from the fact that the direction of movement and speed for all stars are computed based solely on their proper motion data. This calculation then is unreliable for stars with small tangential component because that tends to enlarge their relative error in proper motions and thus their computed parallax ϖ_c. Such stars with small components in tangential motion are stars in the direction of the Galactic Center and the Anticenter. Thus, stars with $340° \leq l \leq 20°$ and $|b| \leq 10°$, as well as stars with $160° \leq l \leq 200°$ and $|b| \leq 10°$ are rejected. Applying all this criteria yields 4253 preliminary candidates, which is 3.6% of *Hipparcos* stars.

To further reduce the number of HVS candidates, we impose the final criterion: we check whether any of these 4253 candidates have radial velocity data from the literatures, and see if it is consistent with the predicted heliocentric radial velocity $v_{R,\mathrm{predicted}}$, calculated by Equation 2.6. We cross-checked the candidates with three different post-*Hipparcos* radial velocity catalogue:

1. The Catalogue of Radial Velocities of Galactic Stars with High Precision Astrometric Data (CRVAD) (Kharchenko, Piskunov, & Scholz, 2004). This catalogue supplements the All-sky Compiled Catalogue of 2.5 Million Stars (ASCC-2.5) (Kharchenko, 2001). It cross-checks entries in the ASCC-2.5 with General Catalogue of Averaged Stellar Radial Velocities (GCRV) (Barbier-Brossat & Figon, 2000) and contains radial velocity data for 34 553 stars, among which 25 413 are *Hipparcos* stars.

2. The Geneva-Copenhagen Survey of the Solar Neighbourhood (Nordström et al. 2004). Whereas the CRVAD contains large number of stars for all spectral type, The Geneva-Copenhagen Survey is a dedicated survey of F and G dwarfs. The radial velocity data was obtained with the CORAVEL spectrometers (Mayor, 1985) and the digital spectrometer (Latham, 1985) of the Harvard-Smithsonian Center for Astrophysics (CfA). The Catalogue contains 16 682 stars, with 14 995 stars with *Hipparcos* entries.

3. Radial velocities for 6691 K and M giants (Famaey et al. 2005). For the purpose of their investigation of the local kinematics of K and M giants, Famaey et al. compiled a list of *Hipparcos* K and M stars complemented with radial velocity data from CORAVEL.

All three catalogues contain entries that overlap with each other. Should there be any overlap, the CORAVEL observations are taken. As a result, 879 radial velocity data are extracted, of which 608 are located outside the direction to the GC and the Anticenter.

To see whether the literature radial velocity $v_{R,\mathrm{literature}}$ is consistent with the predicted radial velocity $v_{R,\mathrm{predicted}}$, its difference $\Delta v_R = |v_{R,\mathrm{literature}} - v_{R,\mathrm{predicted}}|$ is checked whether it is inside the errors of $\sigma_{v_{R,\mathrm{predicted}}}$. 55 stars are within the errors of $v_{R,\mathrm{predicted}}$, however the margin of errors are very large (≥ 1000 km s^{-1}) hence we discard them anyway. The final candidates are 3645 stars, of which the spatial distribution is shown in Figure 3.2. We can see that, aside from the rejected stars in the Center and Anticenter area, all the candidates are distributed in all directions except in the thin area near the Galactic plane in the direction of Galactic rotation and antirotation.

Of the 3645 early candidates, 3301 have smaller computed parallax angle, so most of these stars have to be put in a farther distance than what is inferred from their observed parallax.

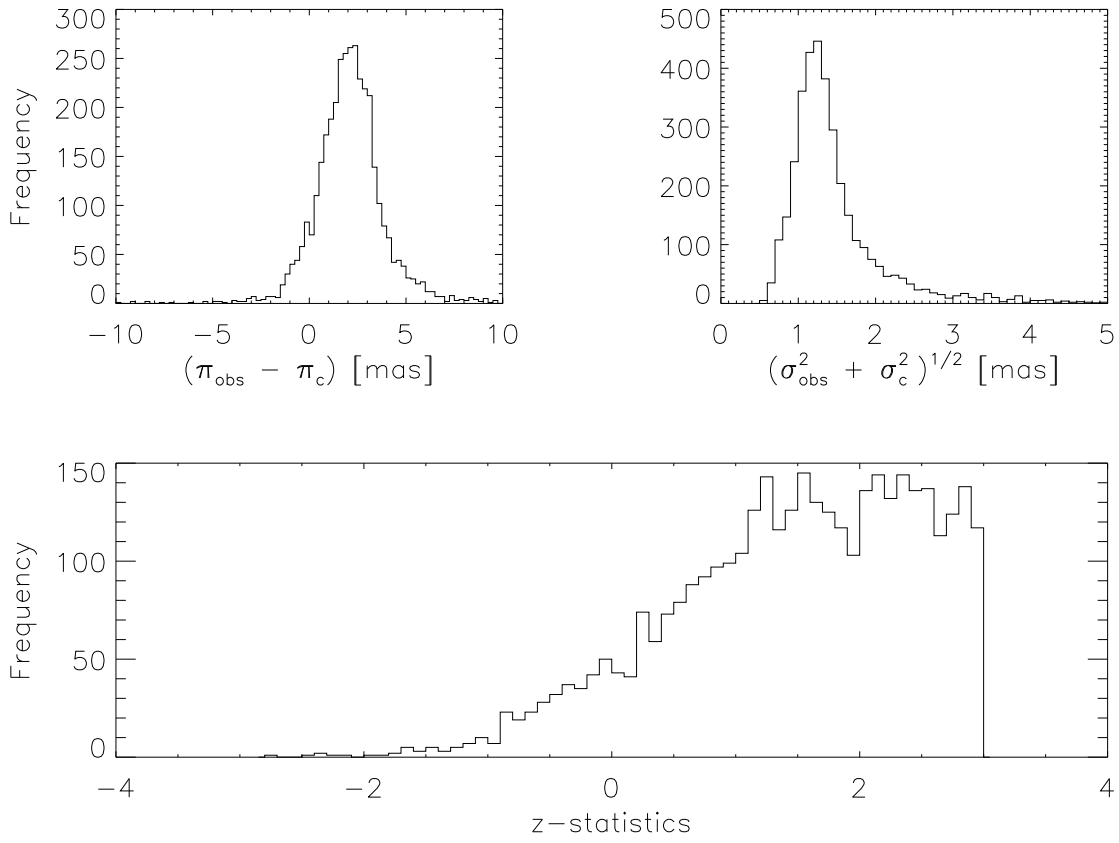

Figure 3.3: Top-Left: The distribution of the difference $(\varpi_{\rm obs} - \varpi_c)$. **Top-Right:** The distribution of the resultant error $(\sigma^2_{\rm obs} + \sigma_c)^{1/2}$. **Bottom:** The histogram for the resulting z values.

This fact is shown in Figure 3.4, which shows a "shift" in the mean observed parallax to smaller values in computed parallax. The rest of it, 344 stars with larger ϖ_c than $\varpi_{\rm obs}$ arise because of the negative values in $\varpi_{\rm obs}$ and their large errors. If we now assume that the computed parallax is the correct distance indicator, then most of these stars would be extremely bright and this is confirmed by their position in the Hertzsprung-Russel Diagram, plotted using the computed parallax ϖ_c, shown in Figure 3.5. As we all can see, most of these HVS candidates are not supposed to exist at all because of their extreme brightness. At the very least, if they really are hypergiants, then they should be extremely rare and we are not expecting those area to be very crowded. These stars get selected because they have larger error in their observed parallax $\varpi_{\rm obs}$ than their computed parallax ϖ_c, hence their absolute differences in parallax is still within 3σ. The number of preliminary candidates, 3645 stars out of 118 218 or 3.08% of the total sample, are still too big for the expected number of HVS that could possibly enter *Hipparcos*' detection

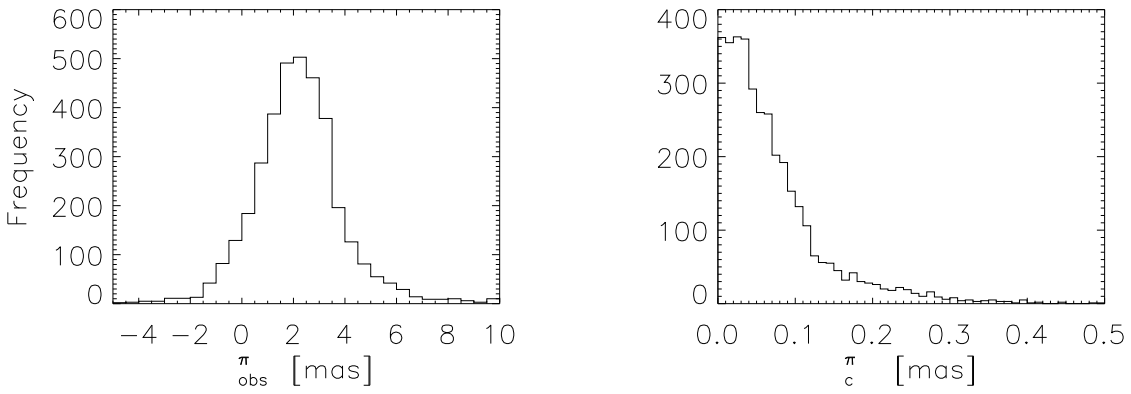

Figure 3.4: Left: The histogram for observed parallax $\varpi_{\rm obs}$ of 3645 early HVS candidates. **Right:** Same as in the left, but for the computed parallax ϖ_c.

sphere. In fact, if theoretical models dictate that there are only ~ 1000 HVS within $\sim 10^{11}$ stars within the solar circle then we should not expect any HVS to be within the solar neighborhood! Large inaccuracies in the astrometric data adds up to this large number of possible candidates. We have to remember that we are looking at objects with low apparent brightness and this makes it difficult to have a reliable astrometric measurement. This fact is shown in Figure 3.6, which shows that errors in measured astrometric parameters increase with apparent magnitude. Also, comparison between the errors in observed parallax and the computed one shows clearly that the resultant error $(\sigma^2_{\rm obs} + \sigma^2_c)^{1/2}$ is dominated by the errors in the observed parallax rather than the errors in the computed one, which is a function of the errors in proper motion. But as stated before, to this date there are no better parallax catalogue than *Hipparcos*.

3.2 The probability of the candidates being "normal" stars

At this point, looking at Figure 3.5, we could intuitively say that those stars that are extremely bright can be rejected straightaway just by looking at their absolute magnitude. We can simply make a clear cut for stars with $M_V \leq -6.0$, this will take 2704 stars but there are still 941 stars left where most of them filled up the extremely rare supergiant area of the Hertzsprung-Russell Diagram.

Another way to look at this problem is to see the position of these candidates in the Hertzsprung-Russell Diagram, relative to the stars with better measurement in parallax (the so-called "good" stars, colored red in Figure 3.5). As we see it in Figure 3.5, we could say that a

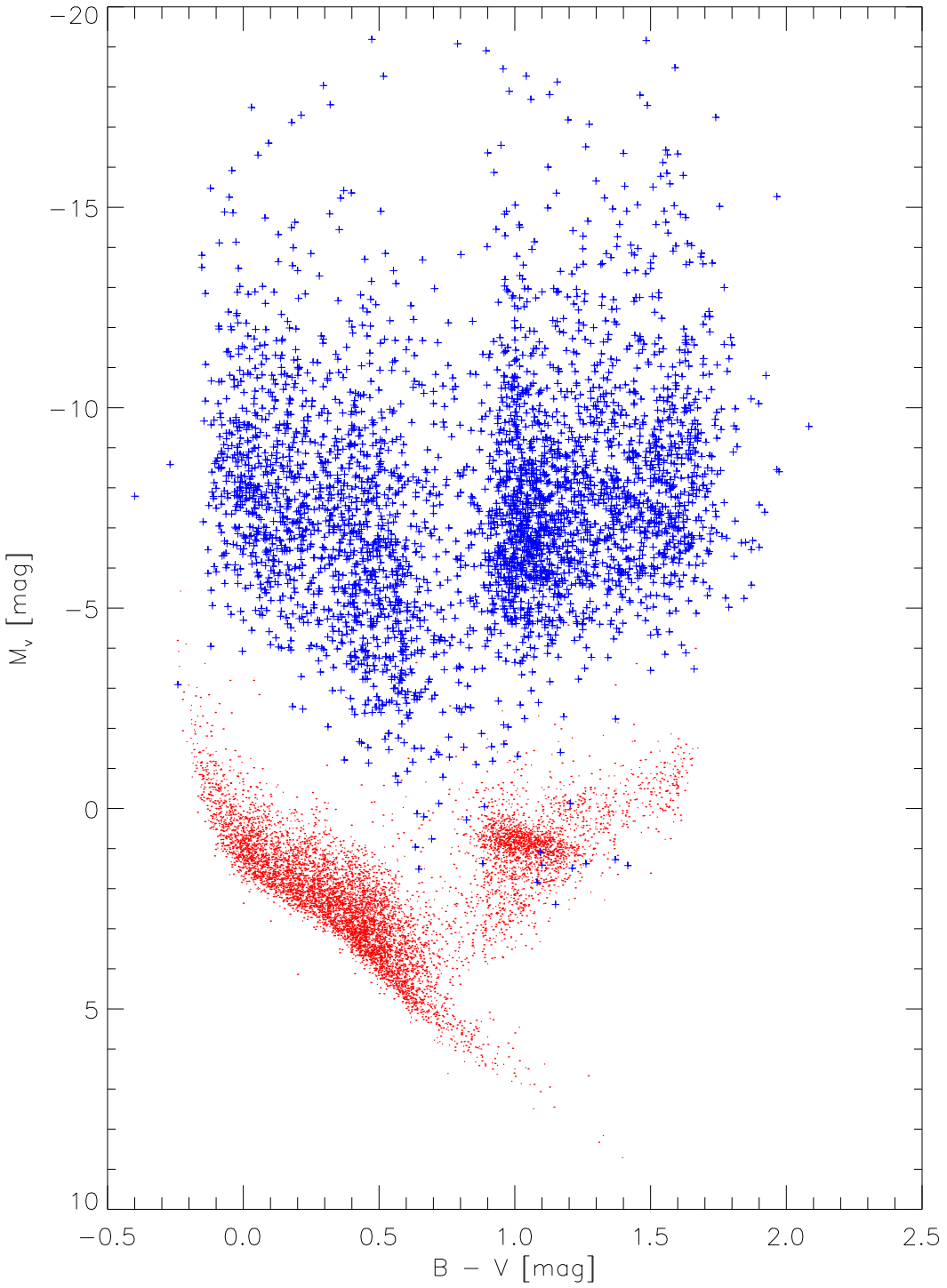

Figure 3.5: The position of 3645 HVS candidates in H-R Diagram (blue). The plot of 8269 *Hipparcos* stars with parallax relative error $\sigma_{\varpi}/\varpi \leq 0.1$ and apparent magnitude $V \leq 7.3$ are also shown (red), as a comparison to the candidates' position in Diagram.

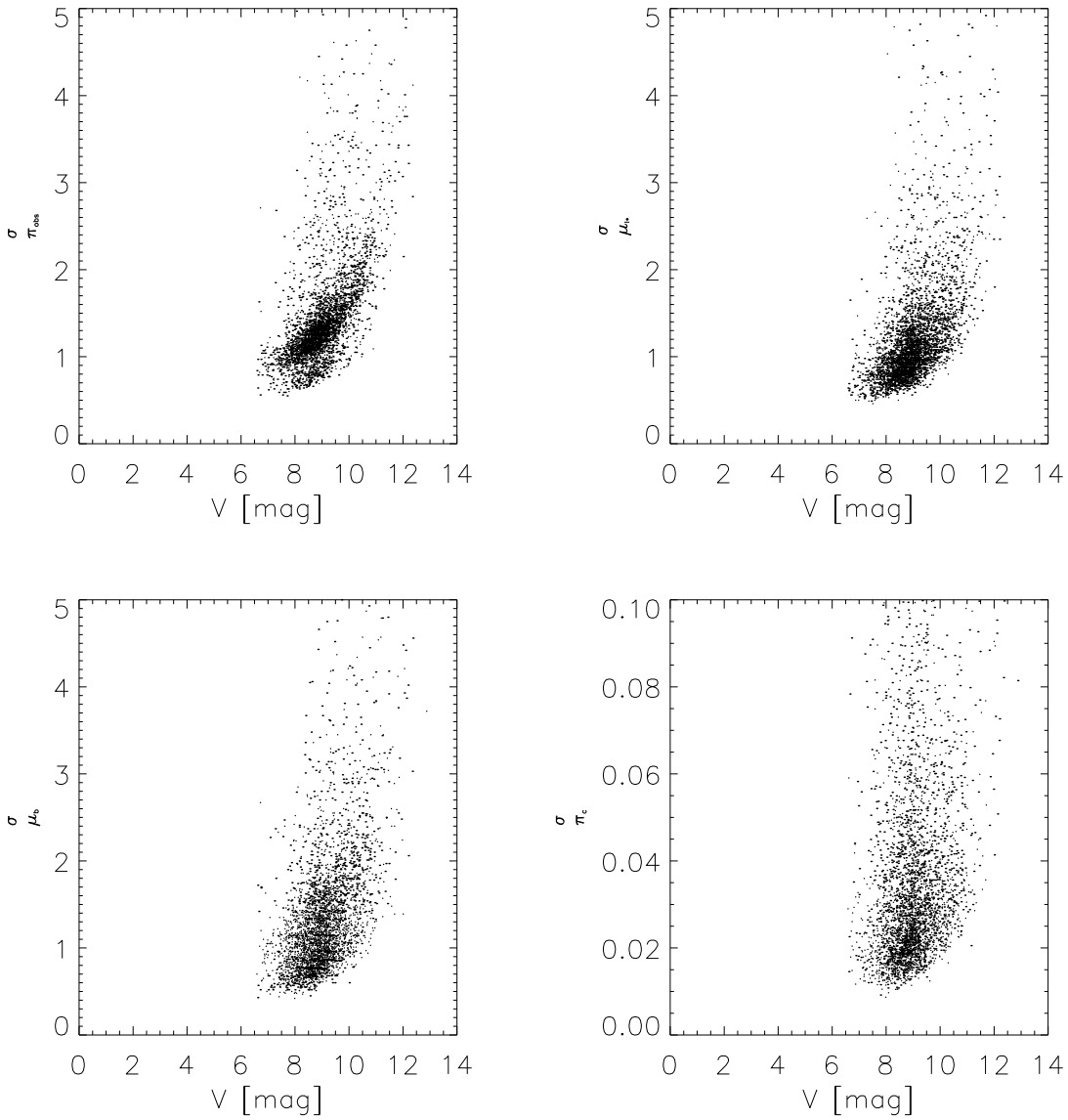

Figure 3.6: The errors in measured astrometric parameters: observed parallax $\varpi_{\rm obs}$ **(top-left)** and the proper motions μ_{l*} **(top-right)** and μ_b **(bottom-left)** (both derived from measured proper motions in equatorial coordinates, $\mu_{\alpha*}$ and μ_δ), as well as the resulting observed parallax ϖ_c **(bottom-right)**.

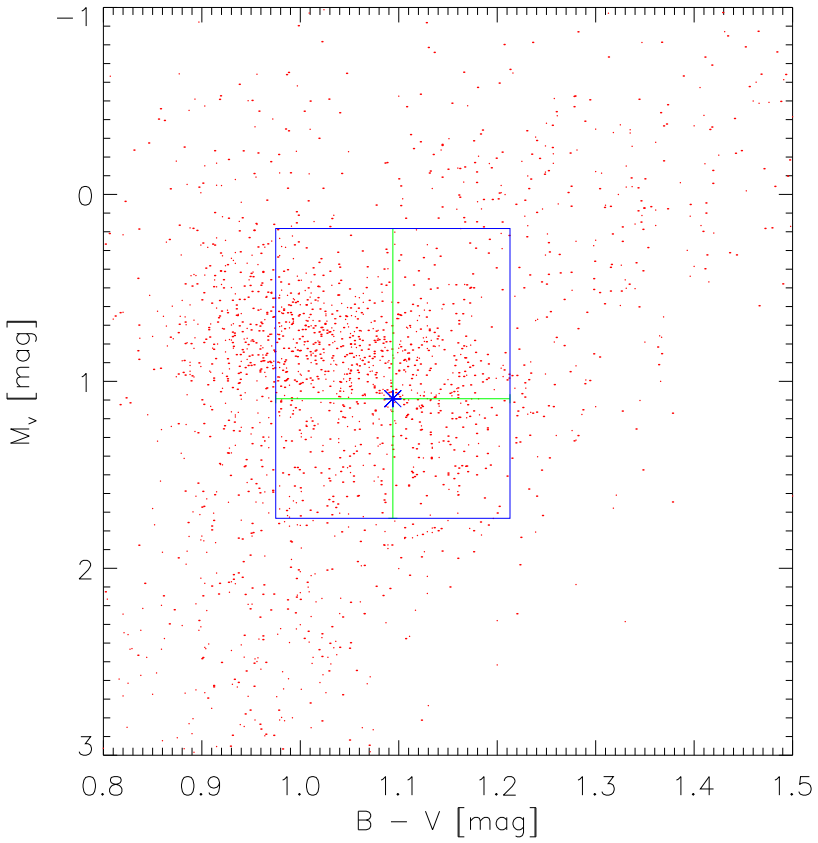

Figure 3.7: An example of an error rectangle. For each candidate with position $(B-V, M_V)$ in the H-R Diagram, an error rectangle is constructed from its errors. Each star will have an error box with width $2\sigma_{B-V}$ and height $\sigma^{+}_{M_V} + \sigma^{-}_{M_V}$. We then calculate the number of red-coloured stars, the so-called "good" *Hipparcos* stars (defined in Section 3.3), and calculate its number density of good stars.

candidate that is located much closer to the bulk of the "good" stars could possibly be a better candidate than the ones that are located much farther.

To elaborate this idea with a mathematical procedure, a method to estimate the probability is devised. In every HVS candidates there are errors in colour index $(B - V)$ and absolute magnitude M_V, derived from errors in ϖ_c. Hence, for every candidates we can construct an error rectangle with a width of $2\sigma_{B-V}$ and a length of $\sigma^+_{M_V} + \sigma^-_{M_V}$ to account for the asymmetric error bars (See Figure 3.7 for an illustration).

We could then count the number of "good" stars within this error rectangle, and next the number density of "good" stars, which is the number of stars within the error rectangle divided by its area. The density of "good" stars within the error rectangle of each candidates could then become a parameter for its proximity to the area in the Hertzsprung-Russell Diagram that are usually populated by ordinary stars. From this density then we can construct a ranking of the most promising HVS candidates down to the least promising.

3.3 Extracting a subsample of "good" stars from the Hipparcos Catalogue

The crucial thing in calculating the density is in defining the "good stars." It is defined, in principle, as a sample of stars that represent the stellar content of Galactic Center (GC), since we want to compare our HVS candidates with the stars in the GC. Currently, we have no complete knowledge of the stellar content within the Galactic Center, however if we take a bold step and simplify the situation by assuming that the stars in the Galactic Center are just ordinary stars like the stars in the solar neighbourhood, then we could build such a sample from the catalogue of local stars like *Hipparcos*. Additionally, these must also be a representative of similar stars within the H-R Diagram.

To construct a H-R Diagram representing the stellar content of the solar neighbourhood, we could truncate the *Hipparcos* Catalogue to a sample of stars with the best quality in parallax measurement. A $|\sigma_\varpi/\varpi| \leq 0.1$ is usually the practice. If the median error in V-band magnitude is 0.012 mag (ESA 1997, vol. 1, p. xv) and the cut-off in parallax relative error is 10%, that would make the largest error in absolute V-band magnitude M_V to be $\sigma_{M_V} \simeq 0.23$ mag. This is good enough for our purpose, and the small relative error makes the nonlinearity bias (discussed later in Section 3.4) negligible. The 10 percent cut-off automatically exclude the farthest stars and leaves us with 20 812 of the total 118 218 stars in *Hipparcos*, and we have an incomplete

parallax-limited sample at $\varpi = 4.55$ mas.

This 10 percent cut-off will lead, however, to the truncation bias. A truncated sample according to an upper limit in $|\sigma_\varpi/\varpi|$ tend to favour nearby stars or—in other words—stars with large parallax. This cut-off will also favour only the brightest stars since for a given ϖ, the precision σ_ϖ is mainly due to photon noise (Arenou & Luri, 1999). This truncation problem can only be solved with a complete parallax-limited sample down to the faintest possible luminosity, but as of today no such sample exist. The only reliable way to create an unbiased representation of the H-R Diagram is then to impose an apparent magnitude limit. Depending on Galactic latitude b and spectral type, *Hipparcos* is complete to $V = 7.3 - 9$ magnitude, (ESA 1997, vol. 1, p. 4). If we take a simple magnitude cut-off at $V = 7.3$, we obtained a final subsample consist of 8269 stars with $(|\sigma_\varpi/\varpi| \leq 0.1) \cap (V \leq 7.3)$. A comparison between the two definition of "good" stars are shown in Figure 3.8. Green dots are *Hipparcos* stars selected by $(|\sigma_\varpi/\varpi| \leq 0.1)$, while red dots are stars with criteria $(|\sigma_\varpi/\varpi| \leq 0.1) \cap (V \leq 7.3)$. The magnitude cut-off clearly throws out the low-luminosity end of the H-R Diagram, but the early-type stars and the giant branch are intact, and this is the part we are most interested in because most of the promising candidates are located in that area (Figure 3.5). We shall also see later in Section 3.4 that if we use both definition of "good" to estimate the probability of candidates, the resulting ranking does not actually change too much.

3.4 Nonlinearity bias and the Astrometry-Based Luminosity

The non-linear relationship between absolute magnitude M with parallax ϖ will induce biased estimate of absolute magnitude. While a particular star with observed parallax ϖ_0 and error σ_{ϖ_0} would have a Gaussian probability distribution centered at ϖ_0, the derived M_0 from the relation $M_0 = m + 5\log\varpi_0 + 5$ will produce an asymmetry in the error distribution of M, and thus a biased estimate of M_0. The same case also applies for the derived distance $d_0 = 1/\varpi_0$. If we calculate the distance d_0 to the star from its measured parallax by $d_0 = \frac{1}{\varpi_0}$, then the PDF $P(d)$ transforms according to (Trumpler & Weaver, 1953)

$$P(d) = \left|\frac{\partial d}{\partial \varpi}\right| P(\varpi), \tag{3.2}$$

and similarly, $P(M_V)$ transforms according to

$$P(M_V) = \left|\frac{\partial M_V}{\partial \varpi}\right| P(\varpi). \tag{3.3}$$

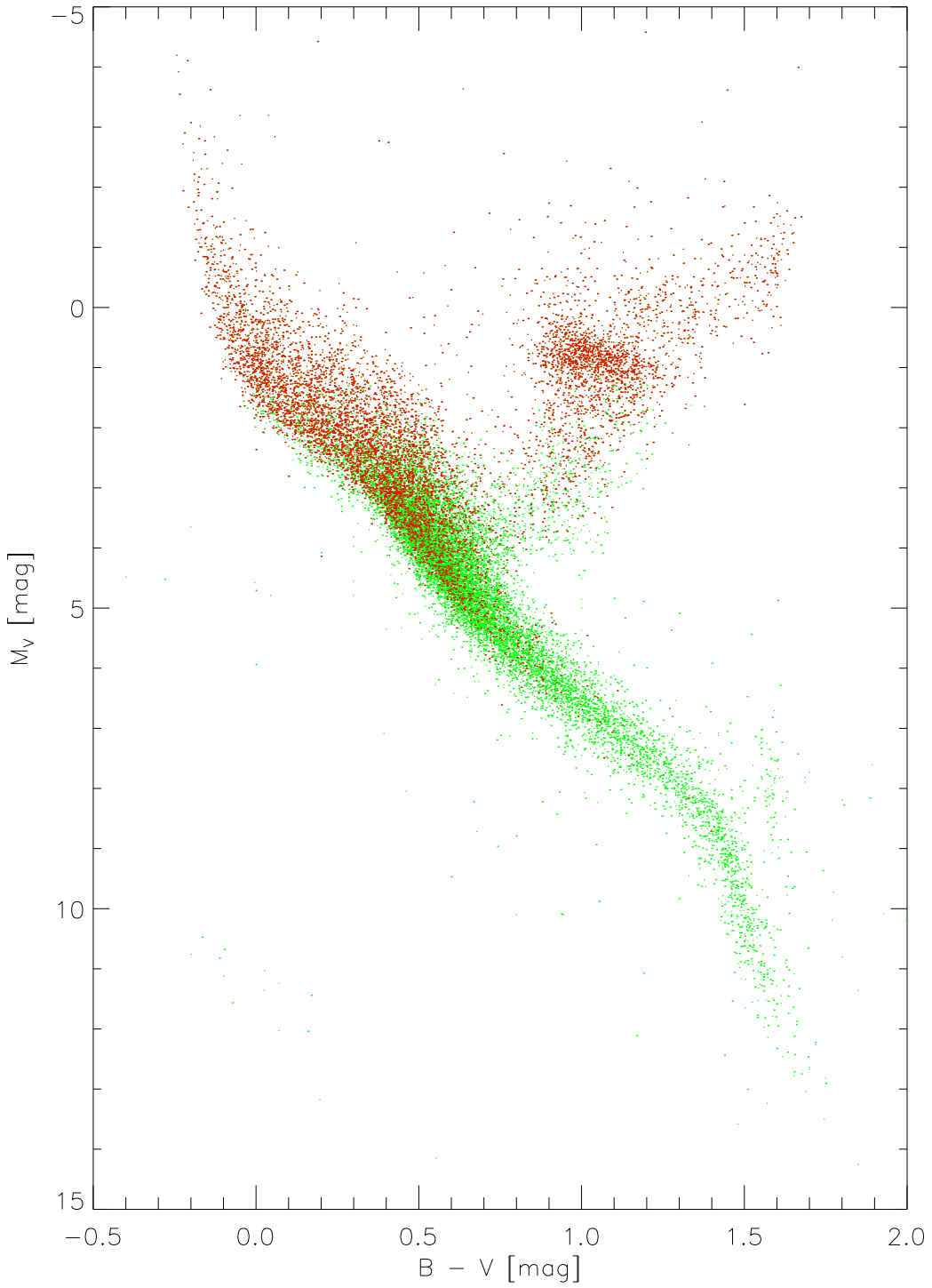

Figure 3.8: The H-R Diagram plot comparing two different subsample of "good" stars: *Hipparcos* stars with only $|\sigma_\varpi/\varpi| \leq 0.1$ **(green dots)** and *Hipparcos* stars with $(|\sigma_\varpi/\varpi| \leq 0.1) \cap (V \leq 7.3)$ **(red dots)**. The magnitude-limited subsample clearly throws out the low-luminosity end of the H-R Diagram.

This will give the Gaussian PDF an additional non-linear factor that depends on ϖ. As an illustration, the calculated PDF for d_0 and M_0 and their sensitivity to errors are given in Figure 3.9. If we have, for example, a parallax measurement for 3 stars with the same mean value of parallax $\varpi_0 = 5$ mas but with three different relative errors $\sigma_{\varpi_0}/\varpi_0 = 0.2, 0.4, 0.5$. The PDF $P(\varpi)$ of the measured parallax (assumed to be Gaussian) for each star is shown in the top-left part of Figure 3.9. From the PDF of d_0 (top-right part of Figure 3.9) we can see that our estimate for d_0 is biased toward the closer distance from us. The curve do not have a Gaussian nor symmetric error distribution and the mean distance d_0 has an offset from the peak distribution, as shown by the dashed line. As the parallax relative error increase, the PDF gets more asymmetric and curve upwards in increasing distance and the bias toward increasing distance gets larger. The same case also applies to the derived absolute magnitude $M_0 = m + 5\log\varpi_0 + 5$, derived by Equation 3.3. For this illustration we use an arbitrary value of apparent magnitude $m = 7.3$ and assume that its measurement errors are negligible. The PDF of M_0 is shown in the bottom-left part of Figure 3.9. The mean absolute magnitude, $M_0 = 0.79$, also has an offset from the peak distribution, and the larger the relative error, the harder it is to correctly estimate its luminosity. We can see that our estimate of M_0 is biased toward fainter magnitude. For larger parallax relative error, the situation is worsening and the bias gets higher up to a point where our estimate of M_0 is useless. Note that it is not the value of σ_{ϖ_0} nor ϖ_0 that matters in the nonlinearity bias, but rather the parallax relative error $|\sigma_\varpi/\varpi|$. We could try the same exercise for other values of ϖ_0 and σ_{ϖ_0} but it is their relative value that will dictate the size of the bias.

The nonlinearity bias in M_0 can be quantified by calculating $E[M_0|\varpi_0] - M$, which is the difference between the expectation value of M_0 with the "true" absolute magnitude M, which we don't know. The value for this bias is (Arenou & Luri, 1999)

$$E[M_0|\varpi_0] - M = \frac{5}{2\pi}\int_{-\infty}^{+\infty} \log\left(1 + u\frac{\sigma_{\varpi_0}}{\varpi_0}\right)\exp(-\frac{u^2}{2})du. \tag{3.4}$$

The bias will be negligible for small relative errors ($\sigma_{\varpi_0}/\varpi_0 \lesssim 0.1$), but it will be 0.2 magnitude brighter when $\sigma_{\varpi_0}/\varpi_0 \sim 0.5$, and rise dramatically for large error. At 200 percent relative error the bias will be 0.6 magnitude too faint (Brown et al. 1997). This large nonlinearity bias at large relative error is, however, the kind of problem we are facing at this moment because the majority of our HVS candidates have large relative error in parallax, as shown in Figure 3.10. $\sim 64\%$ of our candidates have larger than 40% relative error in computed parallax, which is no longer negligible. Thus, for the majority of our candidates, this will complicate the calculation

of the mean absolute magnitude and its uncertainty.

If we linearised the luminosity scale so that it is a linear function of parallax, the truncation bias will be reduced and the nonlinearity bias will disappear altogether (assuming that the errors in apparent magnitude is negligible).

Arenou & Luri (1999) suggest such a thing and offer the quantity

$$a_V = 10^{0.2M_V} = \varpi 10^{\frac{V+5}{5}}, \tag{3.5}$$

where ϖ is in arcsec (or $a_V = \varpi 10^{0.2V-2}$ if ϖ is in mas). This quantity, called the astrometry-based luminosity (ABL), is equal to the inverse of the square root of a flux. The derived PDF $P(a_V)$ from $P(\varpi)$ will also be Gaussian and this will make the nonlinearity bias disappear altogether. Furthermore, this will make the error bars due to parallax errors symmetrical. This makes it easier to handle those stars with parallax error larger than the parallax itself.

Of course the physical meaning of the ABL itself is questionable but for this kind of work where we want to compare two or more objects in the luminosity scale, this quantity is extremely useful because of the linear scale and the lack of biases induced by nonlinearity. After the comparison job is done we could always revert back the results to the logarithmic scale. Figure 3.11 is the so-called "astrometric" H-R Diagram, it is equivalent to Figure 3.5, but the ABL is plotted against colour instead of M_V. We can now see that most of the stars occupy a very thin area in the astrometric HRD, between $a_V = 0$ to $a_V \sim 0.2$.

Finally we can now move on to the problem of calculating the probability of a candidate being a "good" star. This probability is defined as the density of "good" stars within the error rectangle, relative to the cumulative density of "good" stars within the error rectangle of all HVS candidates.

To count the density of "good" stars within the error rectangle of a candidate, we first construct an error rectangle centered at $(a_V, (B-V))$ with the width of $2\sigma_{(B-V)}$ and length $2\sigma_{a_V}$. For every stars that have exactly zero errors in $(B-V)$, the errors were artificially raised to the smallest possible error, $\sigma_{(B-V)} = 0.001$ mag, to avoid a zero area for their error rectangle. The next step is then to count the number n of "good stars" within this error rectangle, and then calculate the density ρ of the "good stars" by

$$\rho = \frac{n}{A}, \tag{3.6}$$

where $A = 4\sigma_{(B-V)}\sigma_{a_V}$ is the area of the error rectangle. After the number density of each candidate is counted, cumulative density $\sum \rho$ of all n candidates is then calculated, and thus

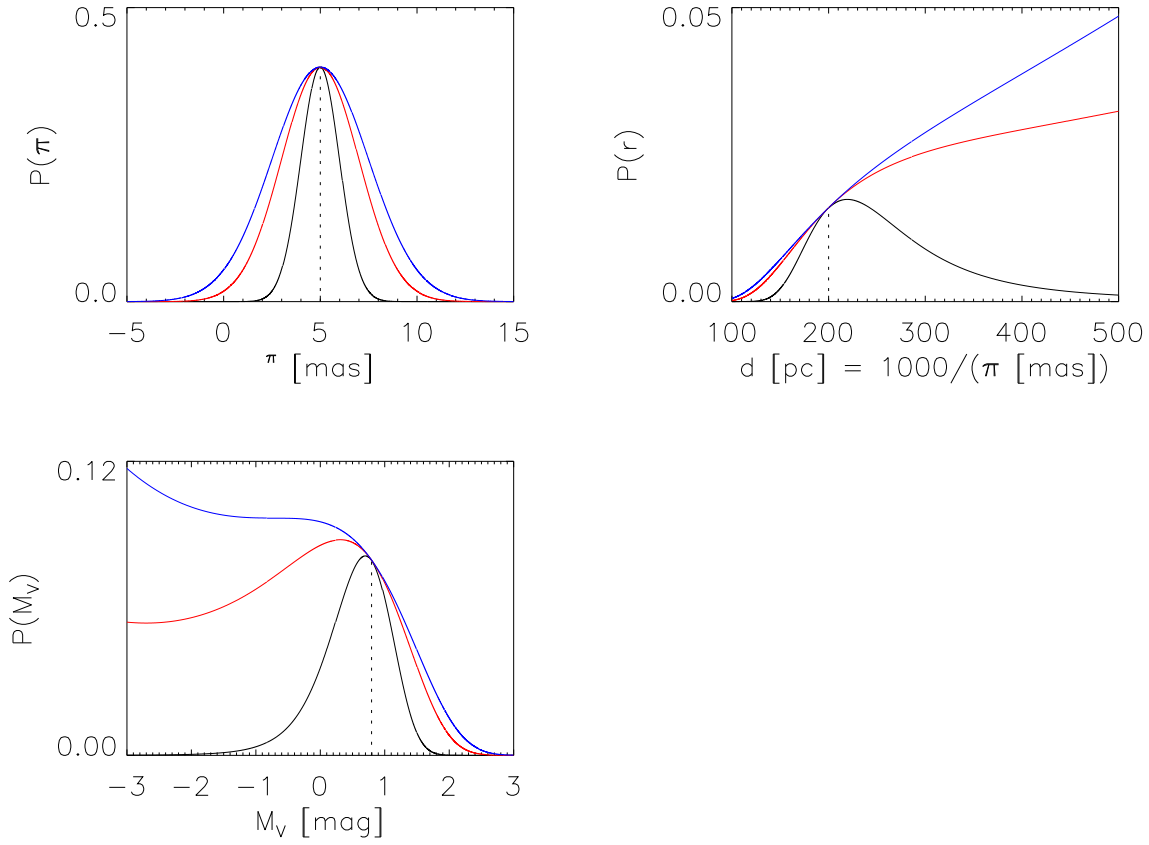

Figure 3.9: The PDF of parallax measurement, and the derived distance and absolute Magnitude, for 3 stars with the same mean parallax $\varpi_0 = 5$ mas but with three different measurement errors: $\sigma_{\varpi_0} = 1, 2, 2.5$ mas, corresponding respectively to relative error $\sigma_{\varpi_0}/\varpi_0 = 0.2, 0.4, 0.5$. The black, red, and blue curve shows the PDF of ϖ_0 and the derived values d and M_0 for the star with $\sigma_{\varpi_0}/\varpi_0 = 0.2, 0.4, 0.5$, respectively. The dashed line shows where the mean parallax $\varpi_0 = 5$ mas is, as well as the derived values. The error distribution of the parallax measurement for each star is assumed to be Gaussian, shown in the **Top Left** part of the Figure. **Top Right:** The PDF for the derived distance from the measured parallax, $d_0 = \frac{1}{\varpi_0}$, calculated by Equation 3.2. **Bottom Left:** The PDF for the derived absolute Magnitude from parallax, $M_0 = m + 5 \log \varpi_0 + 5$, calculated by Equation 3.3.

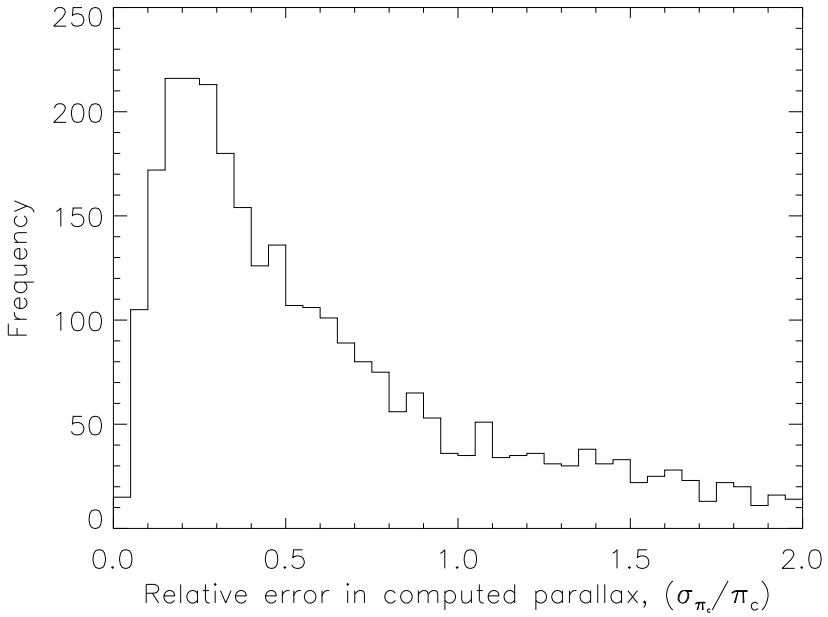

Figure 3.10: The histogram for the relative error in computed parallax ($\sigma_{\varpi_c}/\varpi_c$). $\sim$ 64% of the candidates have relative error ($\sigma_{\varpi_c}/\varpi_c$) larger than 40%

the probability of an i-th HVS candidate being a "good" star is

$$P_i = \frac{\rho_i}{\sum_{i=1}^{n} \rho_i}. \tag{3.7}$$

We apply this technique to our candidates using both subsample of "good" stars. The candidates are then sorted according to decreasing probability using the `quicksort` algorithm in Press et al. (1989). The trend of decreasing probability is shown in the top side of Figure 3.12. Red line is the ranking using "good" sample of HIP stars with only ($|\sigma_\varpi/\varpi| \leq 0.1$), while blue line is the ranking using HIP stars with the magnitude-limited sample ($|\sigma_\varpi/\varpi| \leq 0.1) \cap (V \leq 7.3$). We could also calculate the cumulative probability of the i-th candidate and see how the probability grows with increasing rank. This is shown in the bottom side of Figure 3.12. Beyond the 210th rank the probability is already zero and correspondingly the curve of probability growth shows that there are no growth in probability beyond the 210th rank. Both of curve tell us that there might be only 210 candidates that are worth to be followed-up by further observations, especially radial velocity observations that can be compared with their predicted heliocentric radial velocity given by Equation 2.6. Up until the 10th rank, the probability has already grows to $\sim$50%, so we might say that there might be only 10 "good" candidates. Table 3.1 shows the comparison of the top 20 HVS candidates calculated using the

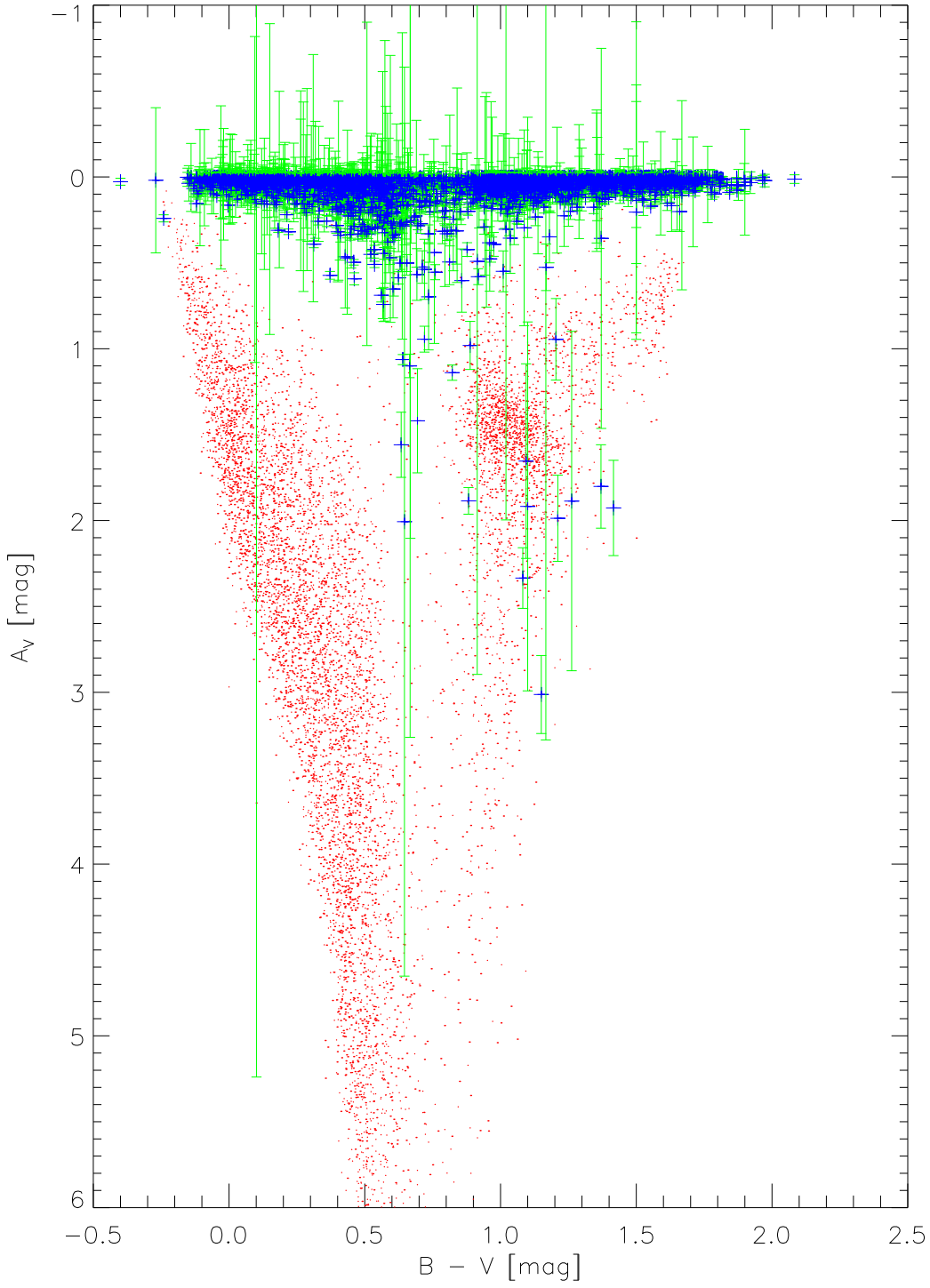

Figure 3.11: The "astrometric" Hertzsprung-Russell Diagram, the ABL, for all HVS candidates and their error bars. This is equivalent to Figure 3.5.

two different subsamples of HIP stars. Rank 1–10 are the same while the rest are just a several steps shift, hence this ranking is actually not sensitive to the accuracy of the representative H-R Diagram.

Finally, Figure 3.13 to 3.15 show both the HR-Diagram and the Astrometric HR-Diagram for, respectively, 15, 50, and 230 top HVS candidates that are ranked using the magnitude-limited subsample of HIP stars. The corresponding top 50 most promising HVS candidates are listed in Appendix C.

Table 3.1: The top 20 HVS candidates, calculated using two different subsample of "good" *Hipparcos* stars: The 10% relative error cut-off and the magnitude limited subsample. Both calculation shows that rank 1–9 is the same while the rest are just shifting between ranks. The ranking technique is not too sensitive to the accuracy of the subsample of "good" stars representing the H-R Diagram in the solar neighborhood.

No.	HIP Number	
	$(\lvert\sigma_\varpi/\varpi\rvert \leq 0.1)$	$(\lvert\sigma_\varpi/\varpi\rvert \leq 0.1) \cap (V \leq 7.3)$
1	36175	36175
2	64945	64945
3	44914	44914
4	62749	62749
5	60553	60553
6	40979	40979
7	106299	106299
8	4327	4327
9	117891	117891
10	89793	66125
11	66125	89793
12	61831	61831
13	64620	32277
14	32277	64620
15	13940	65968
16	65968	73607
17	20968	13940
18	73607	21222
19	21222	114090
20	114090	30950

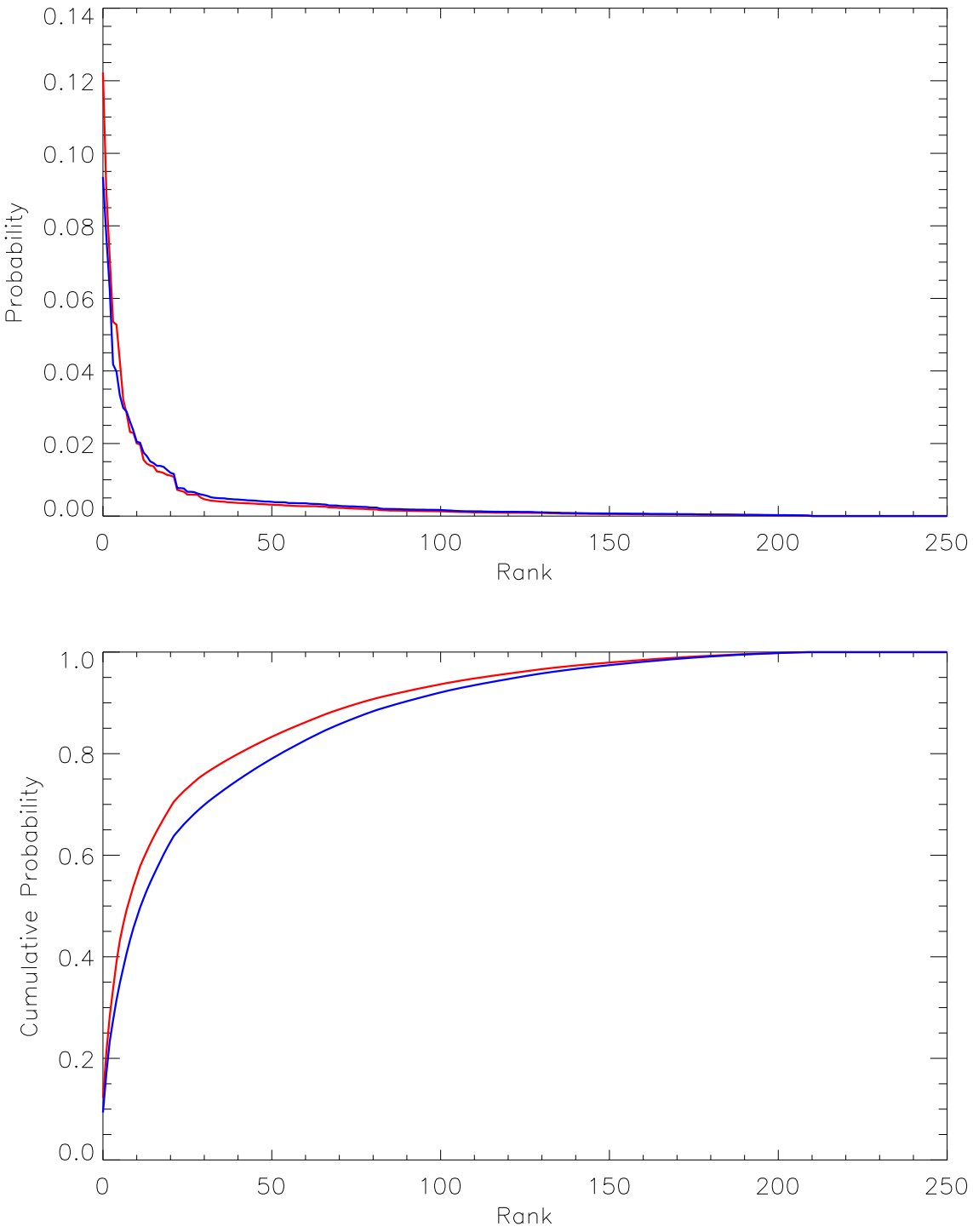

Figure 3.12: Top: The probability plot of each HVS candidates against their respective rank. Red line is the ranking using the "good" sample of HIP stars with ($|\sigma_{\varpi}/\varpi| \leq 0.1$). Blue line is the ranking using the "good" sample of HIP stars with ($|\sigma_{\varpi}/\varpi| \leq 0.1) \cap (V \leq 7.3$). **Bottom:** Same as in the top, but this is the plot of cumulative probability of each candidates against their rank.

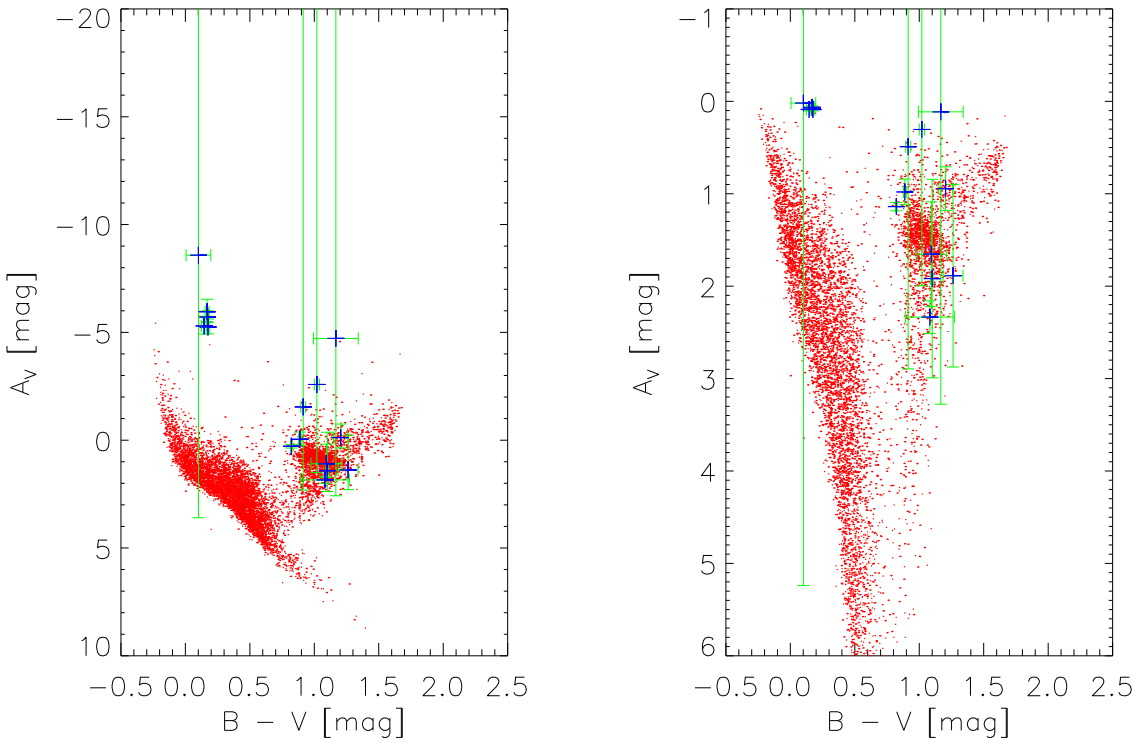

Figure 3.13: Left: HR-Diagram for the top 15 most probable HVS candidates. **Right:** Same as in the left, but in the Astrometric HR-Diagram.

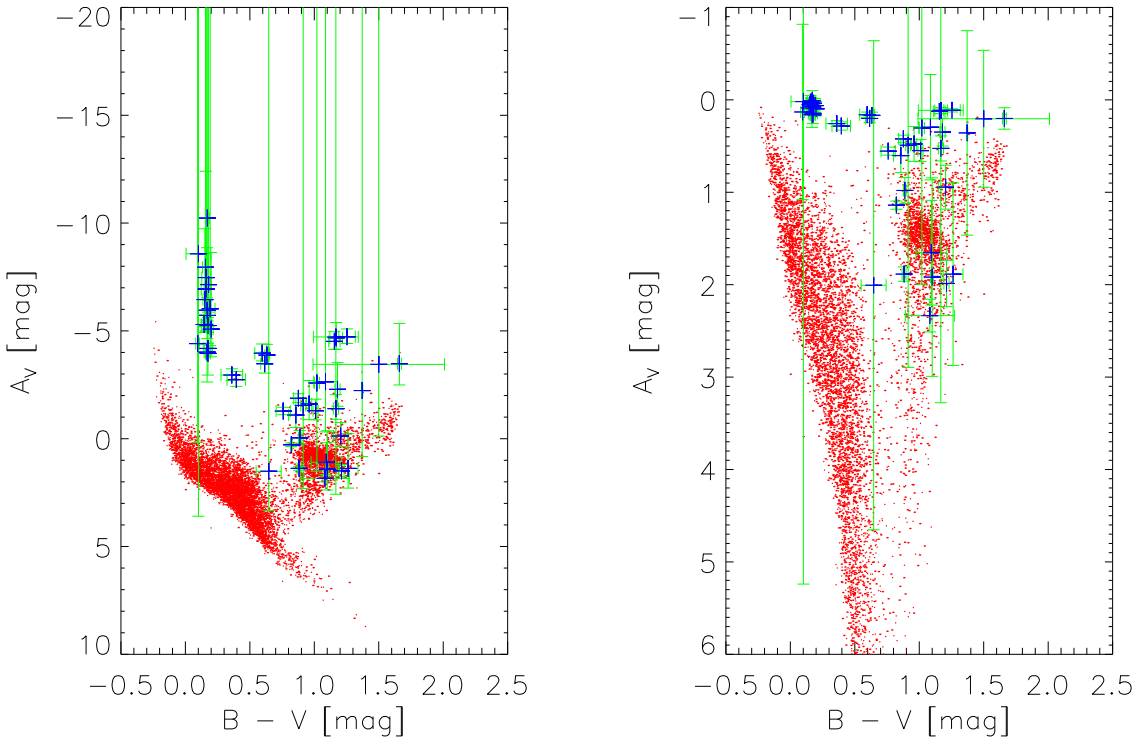

Figure 3.14: Left: HR-Diagram for the top 50 most probable HVS candidates. **Right:** Same as in the left, but in the Astrometric HRD-diagram.

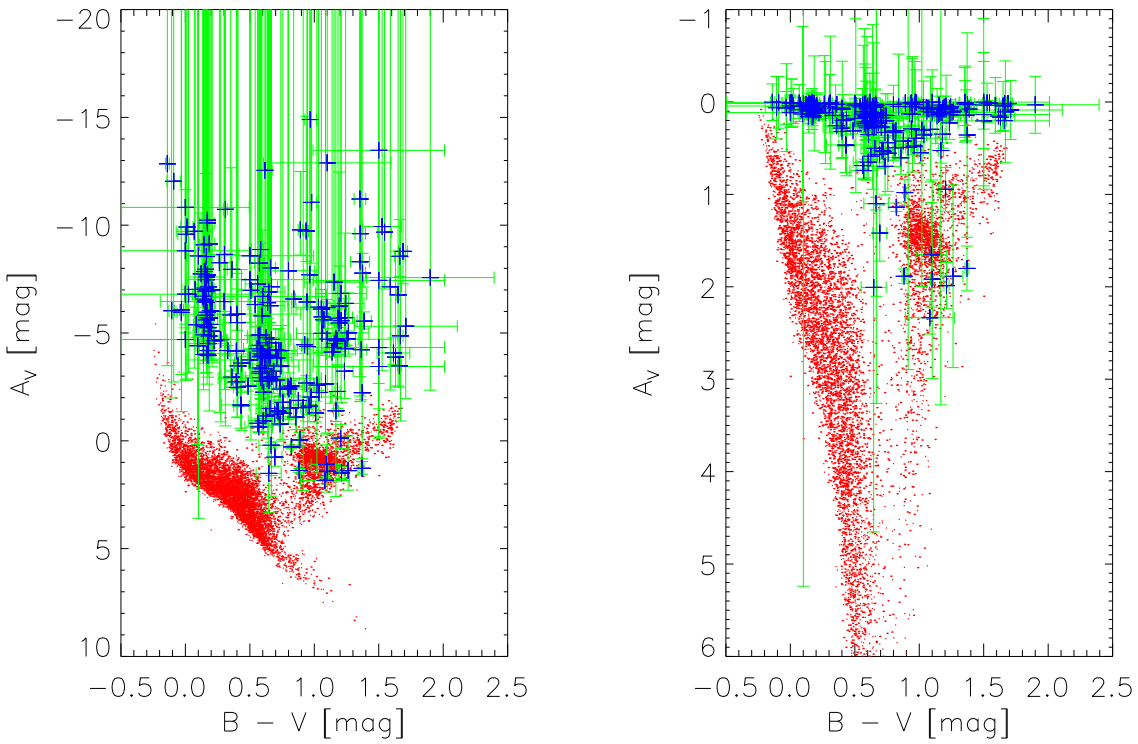

Figure 3.15: Left: HR-Diagram for the top 230 most probable HVS candidates. **Right:** Same as in the left, but in the Astrometric HR-Diagram.

Chapter 4

Discussion

We have demonstrated that we could detect HVS candidates within a large astrometric catalogue, provided we have sufficiently accurate astrometric data. Using three major tests, we try to reject as many stars as possible and produce an observing list that can be followed-up by more thorough observations. As a first test, we checked whether the proper motion of a given star is consistent with the kinematical model of a HVS. This consistency test is manifested in Equation 3.1 where we impose 3σ as the limit. The second test is to check whether the Galactocentric velocity (Equation 2.5) is high enough for the star to be considered a HVS. The final test is whether its position in the H-R Diagram is plausible. To do this we compare our HVS candidates with the "good" stars in the *Hipparcos* Catalogue, as defined in Section 3.3. Several additional rejection criteria are also imposed: Stars with small tangential components as well as any stars with an observed radial velocity that is inconsistent with the predicted one.

The first and second test manage to reject most stars in *Hipparcos*. 5020 stars were selected this way. The fact that the kinematical model of HVS is not correct for the vast majority of stars within *Hipparcos* indicate the extreme scarcity of HVS within the solar neighbourhood, which is already expected. Imposing a loose selection of $(|z| \leq 3.0) \cap (\varpi_c > 0)$ combined with a tighter criterion ($|v_{RF}| \geq 1000$ km s^{-1}) is actually effective in rejecting nearby stars for which we are quite sure that there are no HVS. In fact, this selection brings us straight to the edge of *Hipparcos*' detection sphere where low accuracies and indeterminacy dominate. Applying the aforementioned additional criteria manage to reject more stars and we have 3645 candidates. These candidates have a mean magnitude of $\langle V \rangle \sim 9.$ and mean observed parallax of $\langle \varpi_{\rm obs} \rangle \simeq 2.3$ mas or $\langle \varpi_{\rm obs} \rangle \simeq 2.7$ mas if we exclude candidates with $\varpi_{\rm obs} \leq 0$. This is beyond the completeness limit of *Hipparcos* and took us to areas beyond ~ 400 pc from The Sun. If we

assume that the computed parallax is the correct distance indicator, the mean distance would be even farther at ~ 7.7 kpc from The Sun. We haven't actually exclude candidates moving *toward* the GC, because in itself stars moving toward the GC at extremely high velocity also merit an investigation and explanation. Equation 2.5 preserves the direction of the HVS' movement, and should we choose to exclude all these stars with ($v_{RF} < 0$), then there are 1453 stars to exclude, which leaves us a total of 2192 stars or 1.85% of the total sample.

So far, the first and second test and the additional criteria are actually still not efficient enough. The 3645 HVS candidates is 3.1% of the total sample considered (118 218 stars in *Hipparcos*), although this ratio is small but it is still too big because the expected ratio of HVSs to stars within the solar circle is 10^{-6}%. If we have $\sim 10^9$ stars in our hand and we "only" manage to reject 96.9% of it, then we still have $\sim 3.0 \times 10^7$ stars to sort out! It is clear that we need to develop a more efficient rejection strategy.

By looking at the quantity z that we used as an early criteria, we could see that z is largely determined by the resultant error $(\sigma^2_{\text{obs}} + \sigma^2_c)^{1/2}$, which in turned are connected to the measurement errors of parallax and the proper motion components. Note that low values in z doesn't always mean a high confidence in the candidate because low z could also mean small differences in both the parallax but a high measurement error either in the observed parallax, in the proper motion components, or both. If we look at the table of top 50 HVS candidates in Appendix C, there are still large differences between the observed parallax and the computed one. This is largely due to the large measurement error in the observed parallax. Using a more accurate proper motion catalogue, e.g. Tycho-2 (Høg et al. 2000) or the All-sky Compiled Catalogue of 2.5 (ASCC-2.5) million stars (Kharchenko, 2001) might not help much because the resultant error is dominated by the errors in parallax measurement. The histogram in Figure 3.4 tells us that the mean computed parallax of the sample is 0.08 mas, which is beyond the measuring capability of *Hipparcos* which has a median parallax accuracy ~ 1 mas. We simply need a better parallax measurement if we want to use this technique, and since we have already used the best one available to date then we simply have to wait for the availability of *Gaia* or any other that surpasses *Hipparcos*' mean accuracy in parallax measurement. We are, however, going to face the same problem at the frontiers of *Gaia*'s detection limit. Suffice to say that the first test works efficiently for stars with high astrometric accuracy, but it is problematic for stars with large errors.

The second test, Equation 2.5, is sensitive to the parallax, and in computing this value we adopt the computed parallax as the distance indicator. The accuracy of this test then depends

on the accuracy of the computed parallax which in turn depends on the accuracy of the proper motion measurements.

The *Hipparcos* Catalogue lose its accuracy for faint and faraway stars, a condition we will encounter in the future *Gaia* mission. We then have to resort to a more speculative methods. Our final test, the probability estimate in the H-R Diagram, is devised because we assume that HVS is still a physically normal star although their kinematics is radically different. Hence the usage of a sample of "good" and well-behaved stars from *Hipparcos* to determine whether the candidates are a physically normal star. If we believe that the computed parallax is correct, which we subsequently use to determine each candidate's luminosity, then we could see that the most plausible candidates are the ones that don't stray too far from the H-R Diagram. This procedure, of course, is sensitive to the computed parallax accuracy and the sample of "good" stars that are used. We use two different subsample of "good" stars in this work to see the sensitivity of the ranking to the subsample, the first is a simple 10% parallax relative error cutoff and the second is the magnitude-limited subsample $(\sigma_{\varpi}/\varpi \leq 0.1) \cap (V \leq 7.3)$. The ranking of the candidates from 1 to 9 are the same for both subsample, while the rest just shift up or down several rank, surprisingly this method is not sensitive to the accuracy of the representative H-R Diagram. However, this method could still be improved if we could produce a representative H-R Diagram for the stellar content within the central parsecs of the Galaxy.

The three test relies mostly on the accuracy of the parallax measurement, so a more reliable distance indicator could replace poorly measured parallax, and photometric distance can be a possible replacement. *Gaia* will also conduct a multi-band photometry for all stars, which will make the photometric distance indicator be very well-calibrated by using *Gaia* stars with excellent parallax. Since errors in parallax measurement will be replaced by errors in photometric distance which depends on the errors in photometry, then it is necessary to study how the errors in photometric measurement propagate to the photometric distance.

Another rejection strategy that we could use is a colour selection, but is it an effective criterion? Looking at the fact that most of the currently known HVS are bright early type stars (Brown et al. 2006b) that are presumably young, we must remember that these stars were discovered serendipitously in a pre-targeted survey and the subsequent search is also a targeted search in a tight group of certain stellar type. Although the majority of stars in the Galactic Center might be early type stars, we must not restrict our search only to a certain colour index of star if we remember that at present we still haven't got a complete knowledge on the stellar content of the GC. For simplicity, if we assume that the stellar content within the GC is

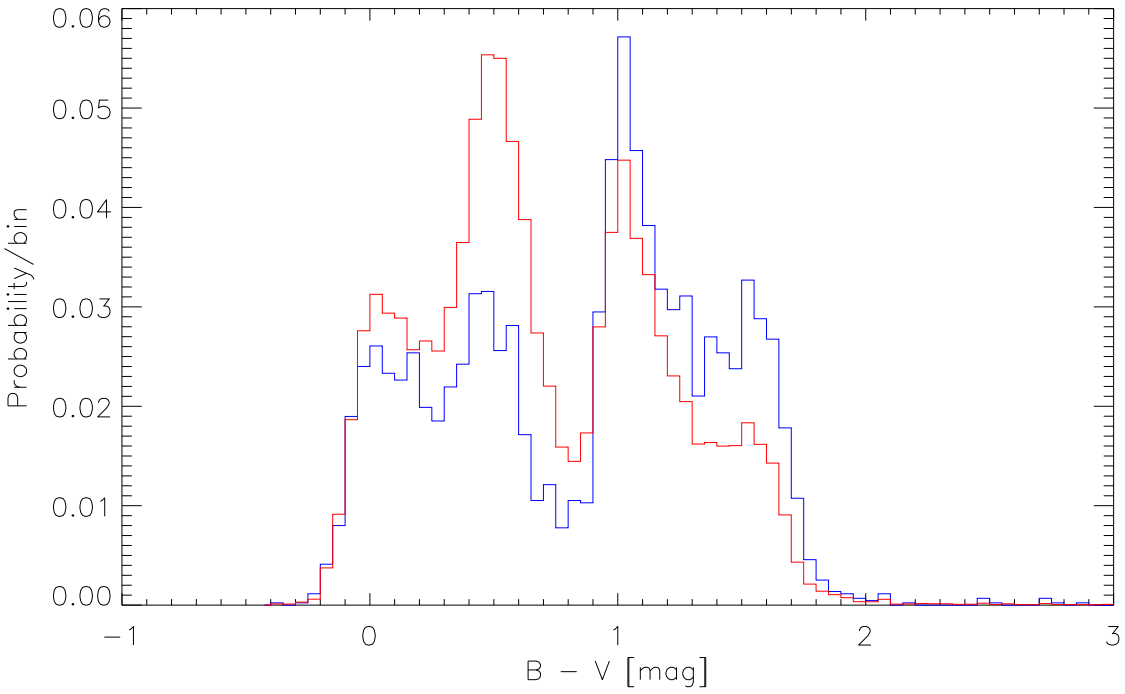

Figure 4.1: The colour distribution of HVS candidates **(blue line)**, compared with the colour distribution of all stars in *Hipparcos* **(red line)**. The vertical axis are the probability per bin size, set at 0.05 mag.

approximately the same as in the solar neighbourhood, old-population and late type HVS might even be more common than the earlier-type HVS. Using samples from *Hipparcos*, Kollmeier & Gould (2007) find that turnoff stars (defined as stars having having absolute magnitude $0.35 < M_V < 4.5$ and near-turnoff colour $0.3 < B_T - V_T < 0.8$, where the subscript T denotes the passband used by Tycho, *Hipparcos*' star mapper) are ~ 67 times more common than B stars, and hypothesised that there could be 1 turnoff HVS in every 10 deg^2 of the sky. Looking at the colour distribution of the HVS candidates in Figure 4.1, and comparing it with the colour distribution of all *Hipparcos* stars, so far the developed criteria also didn't produce any selection to particular colour and in fact the colour distribution of the HVS candidates approximately mirrored the colour distribution of all *Hipparcos* stars. Kollmeier & Gould (2007) also argued that old HVS should also be abundant if HVS are typical of bulge stars. Any criterion based on colour selection then should be based on our best knowledge of the stellar content in the GC.

The list produced from this work in Appendix C has been followed-up by direct observations. Spectra of 7 HVS candidates were obtained on the night of 2007 May 5–6 with the EEV10

camera on the Intermediate Dispersion Spectrograph (IDS) mounted on the 2.5m Isaac Newton Telescope (INT) at Observatorio del Roque de los Muchachos, La Palma, Canary Islands. The H1800V holographic grating was used, it has an 1800 lines mm^{-1} grating, 23.2 Å mm^{-1} dispersion, the central wavelength is selected to be at 4750 Å, with the resolving power $R = 8000$. A cross-correlation of the arcs found that the spectrograph has a variation of zero point by less than $\sim$ 10km s^{-1}, and the cross correlation signal between G and K stars give velocity precision to the order of 1 km s^{-1}. HIP 38984 (No. 31 in the list), 40979 (No. 6), 49857 (No. 29), 57725 (No. 42), 61831 (No. 12), 64945 (No. 2), and 73607 (No. 16) were all observed by cross-correlating them with a normal reference star. All were found to be ordinarily moving stars and do not have the extremely high radial velocity as predicted by the kinematical model (Column 15 on the table in Appendix C) (Le Poole, private communication). The radial velocity precision at the level of IDS is enough to confirm HVS candidates, since most of the candidates have out of ordinary predicted radial velocity thus it will be easy to identify them. Exceptions to this are several stars with small velocity components in their line of sights, i.e. HIP 60553 (No. 5) or HIP 117891 (No. 9). But even for these apparently-slow moving stars, the precision is enough.

Is there a success parameter for this kind of study? Assuming that a fraction of 10^{-6}% HVS among the number of stars in the Galaxy is correct there should be no HVS within *Hipparcos* detection sphere and we aren't expecting that even one of the top 230 stars in our list will turned out to be genuine HVS. This work is just a preliminary study to test whether the technique actually works. One of the problem in this early phase is that we don't know whether there are any HVSs within *Hipparcos*' detection sphere so a probability estimate of succesfully finding HVSs is impossible. For the next phase, a realistic simulation of the *Gaia* catalogue with realistic errors, combined with several models of HVS ejection mechanism from the GC will be needed to explore more efficient rejection strategy.

Bibliography

[1] Arenou, F., Luri, X., 1999, *Distances and absolute magnitudes from trigonometric parallaxes*, in Egret, D., Heck, A., editor, *Harmonizing Cosmic Distance Scales in a Post-Hipparcos Era, ASP Conference Series, Vol. 167*, p. 13–32, ASP, San Francisco, CA.

[2] Barbier-Brossat, M., Figon, P., 2000, *Catalogue gènèral de vitesses radiales moyennes pour les ètoiles galactiques*, **A&AS 142**: 217–223.

[3] Binney, J.J., Merrifield, M., 1998, *Galactic Astronomy*, Princeton Univ. Press, Princeton, NJ.

[4] Brown, A.G.A., Arenou, F., van Leeuwen, F., Lindegren, L., Luri, X., 1997, *Considerations in Making Full Use of the Hipparcos Catalogue*, in Battrick, B., editor, *The Hipparcos Venice '97 (ESA SP-402)*, p. 63–68, ESA, Noordwijk.

[5] Brown, W.R., Geller, M.J.G., Kenyon, S., Kurtz, M.J., 2005, *Discovery of an Unbound Hypervelocity Stars in the Milky Way Halo*, **ApJ 622**: L33–L36.

[6] Brown, W.R., Geller, M.J.G., Kenyon, S., Kurtz, M.J., 2006a, *A Successful Targeted Search for Hypervelocity Stars*, **ApJ 640**: L35–L38.

[7] Brown, W.R., Geller, M.J.G., Kenyon, S., Kurtz, M.J., 2006b, *Hypervelocity Stars.I. The Spectroscopic Survey*, **ApJ 647**: 303–311.

[8] Brown, W.R., Geller, M.J.G., Kenyon, S., Kurtz, M.J., 2007, *Hypervelocity Stars.II. The Bound Population*, **in press,** `http://arxiv.org/abs/astro-ph/0701600`.

[9] Dehnen, W., Binney, J.J., 1998, *Local stellar kinematics from Hipparcos data*, **MNRAS 298**: 387–394.

[10] Edelmann, H., Napiwotzki, R., Heber, U., Christlieb, N., Reimers, D., 2005, *HE 0437–5439: An Unbound Hypervelocity Main-Sequence B-Type Star*, **ApJ 634**: L181–L184.

[11] ESA, 1997, *The Hipparcos and Tycho Catalogue, ESA SP-1200*, ESA Publications Division, Noordwijk.

[12] Famaey, B., Jorissen, A., Luri, X., Mayor, M., Udry, S., Dejonghe, H., Turon, C., 2005, *Local kinematics of K and M giants from CORAVEL/Hipparcos/Tycho-2 data*, **A&A 430**: 165–186.

[13] Fuentes, C.I., Stanek, K.Z., Gaudi, B.S., McLeod, B.A., Bogdanov, S., Hartman, J.D., 2006, *The Hypervelocity Star SDSS J090745.0+024507 is Variable*, **ApJ 636**: L37–L40.

[14] Gnedin, O.Y., Gould, A., Miralda-Escudé, J., Zentner, A.R., 2005, *Probing the Shape of the Galactic Halo with Hypervelocity Stars*, **ApJ 634**: 344–350.

[15] Gualandris, A., Portegies Zwart, S., Sipior, M.S., 2005, *Three-body encounters in the Galactic Centre: the origin of the hypervelocity star SDSS J090745.0+024507*, **MNRAS 363**: 223–228.

[16] Hills, J.G., 1988, *Hyper-velocity and tidal stars from binaries disrupted by a massive Galactic black hole*, **Nature 331**: 687–689.

[17] Hirsch, H.A., Heber, U., O'Toole, S.J., Bresolin, F., 2005, *US 708 – an unbound hyper-velocity subluminous O star*, **A&A 444**: L61–L64.

[18] Høg, E., Fabricius, C., Makarov, V. V., Urban, S., Corbin, T., Wycoff, G., Bastian, U., Schwekendiek, P., Wicenec, A., 2000, *The Tycho-2 catalogue of the 2.5 million brightest stars*, **A&A 355**: L27–L30.

[19] Kharchenko, N.V., 2001, *All-sky Compiled Catalogue of 2.5 million stars (ASCC-2.5)*, **Kinematika Fiz. Nebesn. Tel. 17**: 409.

[20] Kharchenko, N.V., Piskunov, A.E., Scholz, R.-D, 2004, *Astrophysical supplements to the ASCC-2.5. I. Radial velocity data*, **AN 5**: 439–444.

[21] Kollmeier, J.A., Gould, A., 2007, *Where are the Old-Population High Velocity Stars?*, **submitted,** `http://arxiv.org/abs/astro-ph/0701350v1`.

[22] Latham, D.W., 1985, *Digital Stellar Speedometry*, in Philip, A.G.D., Latham, D.W., editor, *Stellar Radial Velocities, IAU Coll. No. 88*, p. 5–20, L. Davis Press, Schenectady, NY.

[23] Levin, Y., 2006, *Ejection of High-Velocity Stars from the Galactic Center by an Inspiraling Intermediate-Mass Black Hole*, **ApJ 653**: 1203–1209.

[24] Mayor, M., 1985, *Cross-Correlation Spectroscopy Using CORAVEL*, in Philip, A.G.D., Latham, D.W., editor, *Stellar Radial Velocities, IAU Coll. No. 88*, p. 21–34, L. Davis Press, Schenectady, NY.

[25] Nordström, B., Mayor, M., Andersen, J., Holmberg, J., Pont, F., Jørgensen, B.R., Olsen, E.H., Udry, S., Mowlavi, N., 2004, *The Geneva-Copenhagen survey of the Solar Neighborhood: Ages, metallicities, and kinematic properties of* $\sim 14\ 000$ *F and G dwarfs*, **A&A 418**: 989–1019.

[26] Perryman, M.A.C., de Boer, K.S., Gilmore, G., Høg, E., Lattanzi, M.G., Lindegren, L., Luri, X., Mignard, F., Pace, O., de Zeeuw, P.T., 2001, *GAIA: Composition, formation, and evolution of the Galaxy*, **A&A 369**: 339–363.

[27] Press, W.H., Flannery, B.P., Teukolsky, S.A., Vetterling, W.T., 1989, *Numerical Recipes: The Art of Scientific Computing (FORTRAN Version)*, Cambridge Univ. Press, Cambridge.

[28] Sesana, A., Haardt, F., Madau, P., 2006, *Interaction of Massive Black Hole Binaries with their Stellar Environment. I. Ejection of Hypervelocity Stars*, **ApJ 651**: 392–400.

[29] Trumpler, R.J., Weaver, H.F., 1953, *Statistical Astronomy*, University of California Press, Berkeley.

[30] Yu, Q., Tremaine, S., 2003, *Ejection of Hypervelocity Stars by the (Binary) Black Hole in the Galactic Center*, **ApJ 599**: 1129–1138.

Appendix A

Coordinate Transform

The position of all stars in *Hipparcos* is described in the equatorial coordinate system of (α, δ), where α is the right ascension and δ is the declination of the star. To put the stars in the context of the structure and dynamics of our Galaxy, it is much more useful to put the stars in a Galactic coordinate system. The Galactic equator is the great circle chosen to be an approximate to the plane of the Milky Way. The plane is inclined at angle of 62.87° to the plane of the celestial equator. The North Galactic Pole (NGP) is located at $(\alpha_{\rm NGP}, \delta_{\rm NGP}) = (192.859\,48°, 27.128\,25°) \simeq (12^{\rm h}51^{\rm m}, +27°7.7')$. The galactic longitude l is measured with respect to the direction to the Galactic Center. The direction to the Galactic Center is then $l = 0°$, $b = 0°$, which corresponds to $(\alpha_{\rm GC}, \delta_{\rm GC}) = (266.405°, -28.936°) \simeq (17^{\rm h}45.6^{\rm m}, -28°56.2')$. Both coordinates for the North Galactic Pole and the Galactic Center are for epoch 2000. The coordinate $(l, b) = (0, 0)$ is also defined by the galactic longitude of the ascending node of the galactic plane on the ICRS celestial equator, which is taken to be $l_\Omega = 32.932\,92°$.

Figure A.1(a) describe the relation between the two coordinate systems. The transform between these two systems, i.e. to transform the coordinates of an arbitrary star from (α, δ) to (l, b), we first define a direction cosine to the star written in terms of equatorial and galactic coordinates:

$$\begin{aligned} \mathbf{r} &= \begin{bmatrix} x_E \\ y_E \\ z_E \end{bmatrix} = \begin{bmatrix} \cos\alpha\cos\delta \\ \sin\alpha\cos\delta \\ \sin\delta \end{bmatrix} \\ &= \begin{bmatrix} x_G \\ y_G \\ z_G \end{bmatrix} = \begin{bmatrix} \cos l\cos b \\ \sin l\cos b \\ \sin b \end{bmatrix}, \end{aligned} \tag{A.1}$$

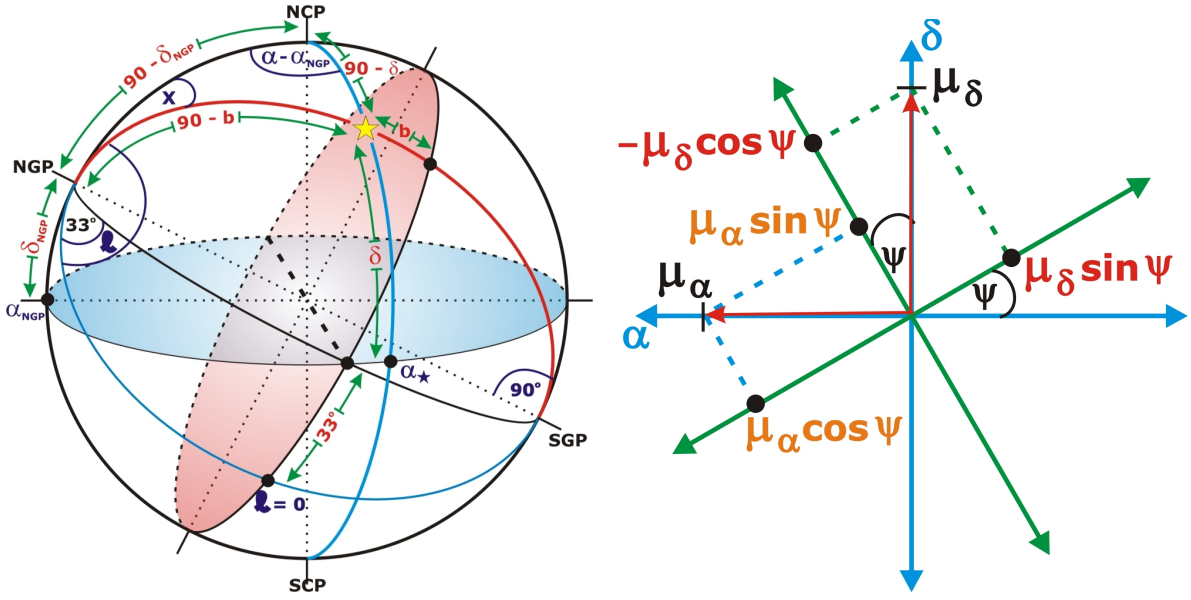

(a) The Galactic and Equatorial coordinate systems

(b) Transformation of proper motions from the Equatorial to the Galactic coordinate system

Figure A.1: (a) An arbitrary star described in the Galactic (l, b) and the Equatorial (α, δ) coordinate systems. NCP is the North Celestial Pole and SCP is the South Celestial Pole. The blue-colored plane is the plane of the celestial equator, while the red-colored plane the plane of the Galactic equator. 33° is approximately the distance from the direction to the Galactic Center $(l, b) = (0, 0)$ to the ascending node. NGP and SGP are the North Galactic Pole and the South Galactic Pole, respectively. **(b)** Transformation of proper motion components $(\mu_{\alpha*}, \mu_\delta)$ in the (α, δ) axis (blue-colored axis) into (μ_{l*}, μ_b) by summation of the projection of $(\mu_{\alpha*}, \mu_\delta)$ to the l and b axis (green-colored axis).

where (x_E, y_E, z_E) is the Cartesian components of the equatorial system. x_E is the component in the direction of $(\alpha, \delta) = (0, 0)$, y_E is in the direction of $(\alpha, \delta) = (90°, 0)$, and z_E is in the direction of $\delta = +90°$. On the other hand, (x_G, y_G, z_G) is the Cartesian components of the Galactic coordinate system. x_G is the component in the direction of the Galactic Center or $(l, b) = (0, 0)$, y_E is in the direction of the Galactic Rotation $(l, b) = (90°, 0)$, and the z_G component is to the direction of the North Galactic Pole or $b = +90°$. The transformation from the Equatorial to Galactic system is given by the relation

$$\begin{bmatrix} x_G \\ y_G \\ z_G \end{bmatrix} = \mathbf{A_G} \begin{bmatrix} x_E \\ y_E \\ z_E \end{bmatrix}, \tag{A.2}$$

where the matrix $\mathbf{A_G}$ is the 3×3 matrix that rotates the Cartesian reference frame in the

Equatorial system to the Galactic system reference frame. To 10 decimal places, it is

$$\mathbf{A_G} = \begin{bmatrix} -0.054\ 875\ 5604 & -0.873\ 437\ 0902 & -0.483\ 835\ 0155 \\ +0.494\ 109\ 4279 & -0.444\ 829\ 6300 & +0.746\ 982\ 2445 \\ -0.867\ 666\ 1490 & -0.198\ 076\ 3734 & +0.455\ 983\ 7762 \end{bmatrix} \tag{A.3}$$

For the transformation of the proper motion components, it is important to remember that the Equatorial and Galactic coordinate system have the same origin. The two axis is inclined by the angle ψ, called the parallactic angle and is an angle between the North Galactic Pole, the star's position, and the North Celestial Pole. The transformation of $(\mu_{\alpha*}, \mu_\delta)$ into (μ_l, μ_b) is done by projecting the proper motion components $(\mu_{\alpha*}, \mu_\delta)$ into the l and b axes so that we obtain the relations between (μ_{l*}, μ_b) and $(\mu_{\alpha*}, \mu_\delta)$ (Figure A.1(b)):

$$\mu_{l*} = \mu_{\alpha*}\cos\delta\cos\psi + \mu_\delta \sin\psi \qquad \mu_b = -\mu_{\alpha*}\cos\delta\sin\psi + \mu_\delta\cos\psi, \tag{A.4}$$

with parallactic angle ψ takes the form

$$\begin{aligned} \cos b\cos\psi &= \sin\delta_{\rm NGP}\cos\delta - \cos\delta_{\rm NGP}\sin\delta\cos(\alpha - \alpha_{\rm NGP}) \\ \cos b\sin\psi &= \sin(\alpha - \alpha_{\rm NGP})\cos\delta_{\rm NGP} \end{aligned}$$

Equation A.4 can arranged into the matrix form

$$\begin{bmatrix} \mu_{l*} \\ \mu_b \end{bmatrix} = \begin{bmatrix} \cos\psi & \sin\psi \\ -\sin\psi & \cos\psi \end{bmatrix} \begin{bmatrix} \mu_{\alpha*} \\ \mu_\delta \end{bmatrix} \tag{A.5}$$

$$\begin{bmatrix} \mu_{l*} \\ \mu_b \end{bmatrix} = \mathrm{J} \begin{bmatrix} \mu_{\alpha*} \\ \mu_\delta \end{bmatrix} \tag{A.6}$$

The 2×2 rotation matrix is a Jacobian that will be useful for further calculations.

Now, to describe the position and motion of stars relative to the Sun, let us first define a right-handed Cartesian frame of reference with the Sun at the orig'in. $\hat{\mathbf{x}}$ is the unit vector pointing to the direction of the Galactic Center ($l = 0°, b = 0°$ in the Galactic Coordinate system), $\hat{\mathbf{y}}$ points to the direction of Galactic rotation ($l = +90°, b = 0°$), and $\hat{\mathbf{z}}$ points to the direction of Galactic Pole ($b = +90°$). Having done with the coordinate transformation, we now define the position of all stars in (l, b) coordinates. $\hat{\mathbf{r}}$ is the unit vector pointing from the Sun to the star, also called the line of sight vector, $\hat{\mathbf{p}}$ is perpendicular to $\mathbf{r}$ and points to the direction of increasing l along the small circle at b, and $\hat{\mathbf{q}}$ is also perpendicular to $\mathbf{r}$ and points to the direction of increasing b along the great circle centered at the Sun and passes through (l, b). These vectors then form the normal triads $\mathbf{p}$, $\mathbf{q}$, and $\mathbf{r}$, where $\mathbf{p} = \mathbf{q} \times \mathbf{r}$ and $\mathbf{q} = \mathbf{r} \times \mathbf{p}$.

Knowing this definition of $(\hat{\mathbf{x}}, \hat{\mathbf{y}}, \hat{\mathbf{z}})$ and $(\hat{\mathbf{p}}, \hat{\mathbf{q}}, \hat{\mathbf{r}})$, we can now construct the relation between them. First of all, $\hat{\mathbf{r}}$ is related to $(\hat{\mathbf{x}}, \hat{\mathbf{y}}, \hat{\mathbf{z}})$ by

$$\hat{\mathbf{r}} = \hat{\mathbf{x}} \cos l \cos b + \hat{\mathbf{y}} \sin l \cos b + \mathbf{z} \sin b\hat{,} \tag{A.7}$$

and $\hat{\mathbf{p}}$ is related to $(\hat{\mathbf{x}}, \hat{\mathbf{y}}, \hat{\mathbf{z}})$ by

$$\hat{\mathbf{p}} = -\hat{\mathbf{x}} \sin l + \hat{\mathbf{y}} \cos l, \tag{A.8}$$

and finally:

$$\hat{\mathbf{q}} = -\hat{\mathbf{x}} \cos l \sin b - \hat{\mathbf{y}} \sin l \sin b + \hat{\mathbf{z}} \cos b. \tag{A.9}$$

It is very useful to collect all these three equations into one single matrix relating $(\hat{\mathbf{p}}, \hat{\mathbf{q}}, \hat{\mathbf{r}})$ with $(\hat{\mathbf{x}}, \hat{\mathbf{y}}, \hat{\mathbf{z}})$:

$$\begin{bmatrix} \hat{\mathbf{p}} \\ \hat{\mathbf{q}} \\ \hat{\mathbf{r}} \end{bmatrix} = \begin{bmatrix} -\sin l & \cos l & 0 \\ -\cos l \sin b & -\sin l \sin b & \cos b \\ \cos l \cos b & \sin l \cos b & \sin b \end{bmatrix} \begin{bmatrix} \hat{\mathbf{x}} \\ \hat{\mathbf{y}} \\ \hat{\mathbf{z}} \end{bmatrix}. \tag{A.10}$$

This is an orthogonal matrix, which means that its inverse is its transpose. Thus we have

$$\begin{bmatrix} \hat{\mathbf{x}} \\ \hat{\mathbf{y}} \\ \hat{\mathbf{z}} \end{bmatrix} = \begin{bmatrix} -\sin l & -\cos l \sin b & \cos l \cos b \\ \cos l & -\sin l \sin b & \sin l \cos b \\ 0 & \cos b & \sin b \end{bmatrix} \begin{bmatrix} \hat{\mathbf{p}} \\ \hat{\mathbf{q}} \\ \hat{\mathbf{r}} \end{bmatrix}. \tag{A.11}$$

Appendix B

The Propagation of Errors

The propagation of error equation is the computation of error of a variable x which is a function of a variable of more, $u, v, \ldots$, each with their own standard deviation $\sigma_u, \sigma_v, \ldots$:

$$x = f(u, v, \ldots). \tag{B.1}$$

Although it is not too exact, but the the most probable value of x is given by

$$\overline{x} = f(\overline{u}, \overline{v}, \ldots). \tag{B.2}$$

In the limit of finite measurements, the variance of x is given by

$$\sigma_x^2 = \lim_{N\to\infty}\left[\frac{1}{N}\sum_{i=1}^{N}(x_i - \overline{x})^2\right], \tag{B.3}$$

and the deviation of $(x_i - \overline{x})$ is related to the forming variables by expanding $(x_i - \overline{x})$ to a Taylor series:

$$(x_i - \overline{x}) \approx (u_i - \overline{u})\left(\frac{\partial x}{\partial u}\right) + (v_i - \overline{v})\left(\frac{\partial x}{\partial v}\right) + \ldots \tag{B.4}$$

By combining Equation B.3 and B.4 we can state the variance of σ_x^2 as a function of $\sigma_u^2, \sigma_v^2, \ldots$ of variables $u, v, \ldots$

$$\begin{aligned}
\sigma_x^2 &\approx \lim_{N\to\infty}\frac{1}{N}\sum\left[(u_i - \overline{u})\left(\frac{\partial x}{\partial u}\right) + (v_i - \overline{v})\left(\frac{\partial x}{\partial v}\right) + \ldots\right]^2 \\
&\approx \lim_{N\to\infty}\frac{1}{N}\sum\left[(u_i - \overline{u})^2\left(\frac{\partial x}{\partial u}\right)^2 + (v_i - \overline{v})^2\left(\frac{\partial x}{\partial v}\right)^2 + \ldots\right. \\
&\qquad \left. +2(u_i - \overline{u})(v_i - \overline{v})\left(\frac{\partial x}{\partial u}\right)\left(\frac{\partial x}{\partial v}\right) + \ldots\right]
\end{aligned} \tag{B.5}$$

We can state the second line in variance σ_u^2 and σ_v^2 as in Equation B.3:

$$\sigma_u^2 = \lim_{N\to\infty}\left[\frac{1}{N}\sum_{i=1}^{N}(u_i - \overline{u})^2\right] \quad \sigma_v^2 = \lim_{N\to\infty}\left[\frac{1}{N}\sum_{i=1}^{N}(v_i - \overline{v})^2\right] \tag{B.6}$$

while the third line is the covariance σ_{uv}^2 defined as

$$\sigma_{uv}^2 = \lim_{N\to\infty}\left[\frac{1}{N}\sum_{i=1}^{N}(u_i-\overline{u})(v_i-\overline{v})\right]. \tag{B.7}$$

With these definitions, the approach for the standard deviation σ_x for x become

$$\sigma_x^2 \approx \sigma_u^2\left(\frac{\partial x}{\partial u}\right)^2 + \sigma_v^2\left(\frac{\partial x}{\partial v}\right)^2 + \ldots + 2\sigma_{uv}^2\left(\frac{\partial x}{\partial u}\right)\left(\frac{\partial x}{\partial v}\right). \tag{B.8}$$

This the equation for the propagation of errors. The first two part in this equation is the variance weighted by the partial differentiation of the variable, while the third part is the multiplication of the deviation u and v, weighted by their own respective partial differentiation. If fluctuations in the measurements of u and v do not have any correlation, then we can expect this part vanishes to zero. This approach is sometimes acceptable so that Equation B.8 become

$$\sigma_x^2 \approx \sigma_u^2\left(\frac{\partial x}{\partial u}\right)^2 + \sigma_v^2\left(\frac{\partial x}{\partial v}\right)^2 + \ldots \tag{B.9}$$

Whenever the covariance is available, this work uses Equation B.8 to compute the error. Otherwise Equation B.9 is used.

Appendix C

The top 50 HVS Candidates

Col.	Description
1	The candidate's rank.
2	HIP Number from the *Hipparcos* Catalogue.
3–4	Position in Galactic Coordinates l and b.
5–6	Apparent magnitude in V-band and the Colour Index, both taken from *Hipparcos*.
7	Absolute magnitude in V-band, calculated using computed parallax ϖ_c and neglecting absorption of the interstellar matter.
8	Astrometry-Based Luminosity (ABL), calculated from Equation 3.5.
9	Observed parallax in miliarcsecond, taken from *Hipparcos*.
10	Computed parallax in miliarcsecond, calculated from Equation 2.4.
11	The z-statistics, calculated from Equation 3.1.
12–13	Proper motion in Galactic Coordinates, transformed from proper motion in Equatorial Coordinates, along with their errors.
14	Galactocentric rest-frame Velocity, in 10^3 km s^{-1}, calculated from Equation 2.5.
15	Predicted heliocentric radial velocity, in 10^3 km s^{-1}, calculated from Equation 2.6.
16	The density of "good" *Hipparcos* stars within the candidate's error rectangle, calculated from Equation 3.6.
17	The probability of the candidate being a "good" star. Calculated from Equation 3.7.

No	HIP	l	b	V	$B-V$	M_V	a_V	$\varpi_{\rm obs}$	ϖ_c	z	μ_{l*}	μ_b	v_{RF}	v_R	ρ	P
		$^\circ$	$^\circ$	mag	mag	mag	mag	mas	mas		mas yr^{-1}	mas yr^{-1}	10^3 km s^{-1}	10^3 km s^{-1}	mag^{-2}	
1	36175	281.7	-22.5	10.52	1.09± 0.12	1.09	1.65± 0.57	10.50± 6.99	1.30± 0.45	1.31	276.95± 7.62	44.27± 7.77	-1.07± 0.41	0.31± 0.08	3363.3	0.093
2	64945	326.8	73.2	9.20	0.17± 0.01	-5.72	0.07± 0.01	1.20± 1.40	0.10± 0.01	0.78	-14.30± 0.88	12.23± 1.02	1.10± 0.15	0.77± 0.03	2770.6	0.077
3	44914	262.1	6.6	11.09	1.10± 0.01	1.41	1.92± 1.07	15.80± 5.74	1.16± 0.65	2.53	-274.95± 4.45	-12.57± 4.54	1.18± 0.68	0.50± 0.09	2250.6	0.063
4	62749	302.9	17.6	10.85	1.20± 0.06	-0.12	0.95± 0.24	13.02± 5.31	0.64± 0.16	2.33	-212.36± 3.80	29.70± 2.95	1.58± 0.37	-0.40± 0.21	1504.3	0.042
5	60553	301.2	-12.3	10.51	1.02± 0.02	-2.58	0.30± 1.69	41.37± 17.45	0.24± 1.34	2.35	-238.66± 19.52	-28.21± 14.35	4.62± 29.49	0.09± 17.27	1433.2	0.040
6	40979	177.2	34.2	9.09	0.17± 0.01	-5.25	0.09± 0.01	3.81± 1.33	0.14± 0.02	2.76	7.59± 0.99	-13.14± 1.77	1.44± 2.80	1.37± 1.30	1198.3	0.033
7	106299	46.5	-38.6	11.86	0.89± 0.01	-0.04	0.98± 0.14	9.65± 3.87	0.42± 0.06	2.39	-113.17± 3.54	49.47± 2.96	-1.38± 0.14	0.27± 0.09	1072.9	0.030
8	4327	123.9	-32.2	7.81	0.17± 0.02	-5.96	0.06± 0.02	5.97± 1.97	0.18± 0.04	2.94	26.70± 2.50	3.96± 1.16	1.01± 0.36	0.65± 0.12	1036.1	0.029
9	117891	63.2	-74.4	10.25	0.82± 0.01	0.28	1.14± 0.04	8.49± 2.64	1.02± 0.04	2.83	-220.68± 2.19	54.88± 2.16	-1.04± 0.04	-0.04± 0.00	938.0	0.026
10	66125	305.2	-14.9	9.31	0.91± 0.02	-1.54	0.49± 2.40	52.09± 39.91	0.68± 3.30	1.28	-365.22± 47.65	-57.22± 46.37	2.72± 16.26	-0.97± 9.92	848.2	0.024
11	89793	318.7	-24.2	11.40	1.08± 0.19	1.84	2.33± 0.18	8.64± 2.64	1.23± 0.09	2.81	-306.37± 2.50	-108.71± 2.49	1.43± 0.17	-0.77± 0.13	737.8	0.021
12	61831	124.8	51.9	8.91	0.14± 0.02	-5.30	0.09± 0.02	2.60± 0.88	0.14± 0.03	2.79	-20.22± 0.86	17.50± 1.03	-1.46± 0.09	-1.26± 0.02	727.6	0.020
13	32277	175.1	16.0	9.78	1.26± 0.08	1.38	1.89± 0.99	29.13± 49.92	2.09± 1.09	0.54	38.03± 45.86	193.07± 69.50	-1.70± 4.07	-1.64± 3.70	631.1	0.018
14	64620	306.0	4.4	10.97	0.10± 0.10	-8.58	0.02± 5.22	16.35± 27.02	0.01± 3.34	0.60	-15.63± 22.66	0.80± 19.94	65.33± 17209.30	65.24± 1102.24	594.6	0.017
15	65968	308.4	5.2	11.01	1.17± 0.17	-4.72	0.11± 3.16	6.50± 10.18	0.07± 1.99	0.62	12.90± 19.61	-1.41± 13.75	-1.66± 35.05	-1.15± 16.69	542.7	0.015
16	73607	23.4	58.5	11.27	1.01± 0.02	-1.30	0.55± 0.12	8.82± 3.21	0.31± 0.07	2.65	-132.93± 2.83	-230.98± 3.45	-4.13± 2.72	0.39± 1.48	524.8	0.015
17	13940	171.1	-44.9	12.10	1.21± 0.02	1.49	1.99± 0.25	9.47± 4.88	0.76± 0.10	1.79	13.47± 4.80	-103.59± 5.33	-1.00± 0.61	-0.78± 0.38	498.5	0.014
18	21222	213.3	-37.9	10.88	1.37± 0.00	-2.23	0.36± 1.11	26.61± 19.70	0.24± 0.74	1.34	171.39± 24.49	-147.93± 20.23	-8.08± 3.95	-6.66± 1.89	497.2	0.014
19	114090	26.0	-66.7	10.30	0.63± 0.01	-3.88	0.17± 0.03	1.28± 1.89	0.15± 0.03	0.60	21.39± 1.83	-54.83± 1.82	2.11± 0.56	0.88± 0.19	486.9	0.014
20	30950	177.7	11.8	8.55	0.17± 0.04	-4.19	0.15± 0.02	-0.02± 1.70	0.28± 0.03	-0.18	15.60± 1.28	-11.03± 1.73	1.22± 1.27	1.21± 0.88	457.3	0.013
21	3298	110.8	-79.2	11.14	0.88± 0.01	1.38	1.89± 0.08	7.77± 2.92	1.12± 0.05	2.28	272.96± 3.32	46.10± 1.80	1.16± 0.06	0.17± 0.00	429.5	0.012
22	11004	141.7	-21.0	8.11	0.15± 0.01	-6.45	0.05± 0.04	4.05± 2.48	0.12± 0.10	1.58	20.77± 2.31	5.91± 2.85	1.83± 2.41	1.58± 0.97	417.1	0.012
23	35516	162.3	25.9	8.83	0.17± 0.02	-3.95	0.16± 0.09	10.56± 6.70	0.28± 0.16	1.53	28.60± 5.54	-20.51± 8.09	1.23± 0.84	1.08± 0.52	277.4	0.008
24	7454	142.4	-54.8	12.13	1.17± 0.02	-1.40	0.53± 0.14	10.69± 3.76	0.20± 0.05	2.79	-13.85± 4.04	-27.41± 3.87	-1.17± 0.65	-0.96± 0.22	276.8	0.008
25	19132	162.6	-13.3	10.21	0.16± 0.01	-6.95	0.04± 0.06	5.06± 1.93	0.04± 0.06	2.60	-2.50± 1.81	-3.24± 2.14	-7.43± 15.99	-7.45± 3.61	273.4	0.008
26	17653	247.6	-51.4	9.74	1.16± 0.04	-4.51	0.13± 0.02	1.63± 1.13	0.14± 0.03	1.32	-24.40± 1.18	13.39± 0.99	1.40± 0.14	1.17± 0.02	240.8	0.007
27	20968	228.7	-42.2	11.42	0.65± 0.10	1.51	2.01± 2.65	120.70± 56.47	1.04± 1.38	2.12	265.68± 61.60	-113.89± 44.28	-1.50± 1.37	-0.72± 0.63	240.6	0.007
28	21603	248.0	-41.9	10.51	0.18± 0.02	-7.15	0.04± 0.05	3.33± 1.24	0.03± 0.04	2.66	-5.25± 1.31	2.39± 1.29	4.35± 3.38	4.41± 0.22	237.5	0.007
29	49857	240.2	43.5	9.02	1.25± 0.06	-4.73	0.11± 0.02	3.52± 1.28	0.18± 0.03	2.61	37.97± 1.17	8.04± 1.15	-1.45± 0.31	-0.93± 0.08	223.9	0.006
30	18971	162.4	-13.8	10.38	0.20± 0.01	-5.08	0.10± 0.08	1.68± 2.07	0.08± 0.07	0.77	9.17± 1.59	3.74± 2.52	2.55± 5.05	2.46± 1.95	214.6	0.006
31	38984	176.1	30.1	10.14	0.76± 0.05	-1.28	0.55± 0.04	2.93± 1.88	0.52± 0.04	1.28	37.60± 1.88	-93.97± 2.21	2.05± 0.85	1.85± 0.61	207.5	0.006
32	93961	11.2	-14.9	12.05	0.96± 0.02	-1.61	0.48± 0.19	3.71± 3.76	0.19± 0.07	0.94	8.50± 2.91	-22.97± 3.93	1.01± 0.44	-0.76± 0.94	199.2	0.006
33	35364	182.9	20.4	9.95	0.36± 0.08	-2.95	0.26± 0.03	0.17± 1.90	0.26± 0.03	-0.05	9.50± 1.68	-21.03± 2.21	1.50± 1.60	1.47± 1.05	185.8	0.005
34	11227	168.2	-56.2	9.10	0.62± 0.03	-3.48	0.20± 0.04	5.24± 4.03	0.31± 0.07	1.22	30.97± 3.33	63.86± 5.04	1.58± 2.06	1.16± 0.90	181.5	0.005
35	28799	159.7	15.2	9.33	0.16± 0.04	-6.92	0.04± 0.04	-1.24± 1.34	0.06± 0.05	-0.97	12.31± 0.96	-6.79± 1.42	7.20± 3.95	7.07± 1.18	178.1	0.005
36	14243	144.3	-8.6	9.42	0.19± 0.04	-6.03	0.06± 0.07	3.22± 1.44	0.08± 0.10	2.17	7.95± 1.11	0.54± 1.32	1.09± 2.39	0.93± 0.83	176.5	0.005
37	40721	249.8	3.0	11.71	0.09± 0.01	-4.41	0.13± 0.95	4.63± 2.65	0.06± 0.43	1.70	-5.91± 2.10	-0.36± 1.79	1.43± 9.62	1.54± 1.33	175.7	0.005
38	51162	199.7	58.3	10.37	0.86± 0.06	-1.10	0.60± 0.18	-10.51± 13.42	0.51± 0.16	-0.82	-10.25± 9.09	-85.77± 12.35	1.02± 1.04	0.69± 0.45	169.7	0.005
39	23227	184.3	-15.4	9.32	0.88± 0.04	-1.87	0.42± 0.04	9.76± 3.47	0.58± 0.05	2.65	17.87± 2.14	33.43± 3.25	1.23± 0.82	1.23± 0.66	168.0	0.005
40	41663	208.5	28.9	11.47	1.18± 0.02	-2.29	0.35± 0.15	6.17± 3.44	0.18± 0.08	1.74	-6.18± 2.78	-14.24± 4.18	1.18± 0.90	1.17± 0.44	165.0	0.005
41	109619	92.3	-13.8	11.81	1.50± 0.51	-3.45	0.20± 0.74	1.35± 3.40	0.09± 0.32	0.37	-11.00± 3.16	-1.25± 4.12	-1.02± 4.03	-1.04± 0.10	164.1	0.005
42	57725	143.0	62.1	11.98	0.17± 0.02	-4.01	0.16± 0.14	4.31± 3.07	0.06± 0.06	1.38	6.72± 2.35	-3.50± 2.24	1.27± 1.30	1.11± 0.20	161.7	0.004
43	42205	221.8	25.1	9.43	1.17± 0.05	-4.68	0.12± 0.03	2.96± 1.54	0.15± 0.04	1.82	-9.35± 1.24	-9.19± 1.41	1.12± 0.42	1.14± 0.17	159.1	0.004
44	41857	169.4	36.3	10.55	0.40± 0.07	-2.74	0.28± 0.04	3.91± 1.96	0.22± 0.03	1.88	16.96± 1.50	-20.36± 2.79	1.14± 0.55	1.00± 0.30	155.8	0.004
45	5254	300.8	-48.5	10.92	1.09± 0.09	-2.64	0.30± 0.57	1.05± 12.73	0.19± 0.37	0.07	-66.25± 13.77	-21.70± 14.47	1.70± 4.75	0.60± 1.64	154.3	0.004
46	110026	101.7	-1.9	8.68	0.17± 0.01	-10.23	0.01± 0.11	1.48± 0.80	0.02± 0.20	1.77	-5.02± 0.63	-0.09± 0.62	-11.31± 134.21	-11.43± 3.81	153.0	0.004
47	22536	177.0	-12.8	9.90	0.60± 0.06	-3.96	0.16± 0.03	5.83± 2.42	0.17± 0.03	2.34	5.51± 1.49	-10.82± 1.78	-2.27± 2.26	-2.25± 1.31	149.1	0.004
48	13138	132.3	10.3	9.40	0.16± 0.02	-7.95	0.03± 0.07	0.82± 1.13	0.03± 0.10	0.69	-1.89± 0.92	0.65± 1.01	-2.41± 3.06	-2.53± 0.48	146.8	0.004
49	118095	101.5	-50.9	11.71	1.66± 0.01	-3.48	0.20± 0.12	-0.72± 3.24	0.09± 0.05	-0.25	-10.24± 3.77	-5.15± 2.10	-1.03± 0.90	-0.97± 0.07	143.5	0.004
50	43926	252.3	11.6	9.36	0.16± 0.03	-7.47	0.03± 0.05	1.47± 1.27	0.04± 0.07	1.12	-4.86± 0.87	-0.81± 0.79	1.99± 3.37	2.11± 0.32	143.3	0.004

Acknowledgement

Working with Anthony Brown, the observer, and Yuri Levin, the theoretician, is a great learning experience as it gives me different sides of opinion in viewing problems. I thank them for the discussions and debates we had and for their supervision and advice for this work. It is a great pleasure to work with them.

Raymond Oonk, Harald Verbraak, and Reinout van Weeren helped me a lot in editing the "Nederlandse samenvatting". They really showed me that dictionaries and electronic translators are not enough to know when to use the right words and how to construct a good sentence in Dutch. You just have to use Dutch more often.

My stay in The Netherlands for the first year of my Master study is funded by the Leids Universiteit Fonds, to which I thank them for the grant they provided as well as the quick decision they made back in June 2006 to give the grant.